JOURNAL OF PETROLOGY | VOLUME 37 | NUMBER 3 | PAGES 521–552 | 1996

F. BEA
DEPARTMENT OF MINERALOGY AND PETROLOGY, CAMPUS FUENTENUEVA, UNIVERSITY OF GRANADA, 18002 GRANADA, SPAIN

Residence of REE, Y, Th and U in Granites and Crustal Protoliths; Implications for the Chemistry of Crustal Melts

A systematic study with laser ablation–ICP-MS, scanning electron microscopy and electron microprobe revealed that ~70–95 wt % of REE (except Eu), Y, Th and U in granite rocks and crustal protoliths reside within REEYThU-rich accessories whose nature, composition and associations change with the rock aluminosity. The accessory assemblage of peraluminous granites, migmatites and high-grade rocks is composed of monazite, xenotime (in low-Ca varieties), apatite, zircon, Th-orthosilicate, uraninite and betafite–pyrochlore. Metaluminous granites have allanite, sphene, apatite, zircon, monazite and Th-orthosilicate. Peralkaline granites have aeschinite, fergusonite, samarskite, bastnaesite, fluocerite, allanite, sphene, zircon, monazite, xenotime and Th-orthosilicate. Granulite-grade garnets are enriched in Nd and Sm by no less than one order of magnitude with respect to amphibolite-grade garnets. Granulite-grade feldspars are also enriched in LREE with respect to amphibolite-grade feldspars. Accessories cause non-Henrian behaviour of REE, Y, Th and U during melt–solid partitioning. Because elevated fractions of monazite, xenotime and zircon in common migmatites are included within major minerals, their behaviour during anatexis is controlled by that of their host. Settling curves calculated for a convecting magma show that accessories are too small to settle appreciably, being separated from the melt as inclusions within larger minerals. Biotite has the greatest tendency to include accessories, thereby indirectly controlling the geochemistry of REE, Y, Th and U. We conclude that REE, Y, Th and U are unsuitable for petrogenetical modelling of granitoids through equilibrium-based trace-element fractionation equations.

KEY WORDS: *accessory minerals; geochemical modelling; granitoids; REE, Y, Th, U*

INTRODUCTION

The geochemistry of rare earth elements (REE), yttrium, thorium and uranium forms the basis for many important methods of igneous petrogenesis. In particular, REE are probably the most extensively used elements for petrogenetic modelling, as each major mineral participating in the genesis of a rock is supposed to leave its own recognizable signature on the REE pattern of that rock (e.g. Haskin, 1979, 1990; McKay, 1989). REE-based modelling was first applied to mantle-related systems, where it has found undeniable success. It was then adopted for crustal systems, despite the fact that crustal rocks always contain REE-, Y-, Th-, U-rich accessory minerals (hereafter called REEYThU-rich minerals), which usually account for an elevated fraction of REE, Y, Th and U contents in bulk rock (e.g. Gromet & Silver, 1983; Sawka, 1988; Bea *et al.*, 1994*a*, 1994*b*) and may therefore disturb or even completely mask the effects produced by major minerals during melting and crystallization (Miller & Mittlefehdlt, 1982; Yurimoto *et al.*, 1990).

Since the recognition that REEYThU-rich accessories may play an important role in controlling the geochemistry of crustal melts (e.g. Watson & Harrison, 1984; Watson, 1988; Watt & Harley, 1993), a considerable amount of work has been done in an attempt to understand their effects. However, this effort has been almost exclusively focused on three minerals: zircon, monazite and apatite. Nevertheless, the variety of REEYThU-rich accessories in granite rocks is neither limited to these three minerals nor are they always the main REE, Y, Th and U

carriers. Perusal of available descriptions of granite rocks as well as our routine scanning electron microscope (SEM) studies on Uralian and Iberian granitoids revealed a plethora of REEYThU-rich minerals whose nature, grain-size, textural position, and hence their presumable influence on the behaviour of REE, Y, Th and U during melting and crystallization, change notably from one rock type to another.

This paper presents the results of a systematic study—by scanning electron microscope (SEM), electron microprobe and laser ablation–inductively coupled plasma mass spectrometry (LA–ICP-MS)—on the residence of REE, Y, Th and U in a variety of samples of granitoids, migmatites and granulites from Iberia, Ivrea–Verbano, the Urals, Kola and Transbaikalia. The research was carried out with three objectives: (1) to study the REE, Y, Th and U composition of major minerals in different geological environments; (2) to learn the nature, abundance, composition, grain-size distribution, textural relationships and associations of REEYThU-rich accessories; (3) to determine the relative contributions of major and accessory minerals to REE, Y, Th and U budgets in granitoids and common crustal protoliths.

Based on these results, we address the behaviour of REE, Y, Th and U in granite melts, the role of accessories during crustal melting, melt segregation and crystallization, the effects of pressure on the REE composition of restitic minerals and hence of melts, the influence of accessories on the contrasting geochemistry of REE, Y, Th and U in different granite types, and the mobility of these elements during post-magmatic stages. We then examine the question of whether REE-based petrogenetic modelling of granite rocks—understood as a method for inferring the behaviour of major minerals during melt and crystallization—makes sense or not.

SAMPLES AND METHODS

Samples

About 150 samples from 38 different geological units were selected for this work (Table 1). Slides for thin sections (optical, SEM, microprobe and LA–ICP-MS analyses) were cut from each sample. Crushing of 5–10 kg of rock to a grain-size of <5 mm was done in a crusher with hardened steel jaws adjusted to an output size of 5 mm. Powders for chemical analysis were obtained by grinding about 50 g per sample of crushed rock in a tungsten carbide jar until grain-size was <25 μm. This system produced no detectable contamination with REE, Y, U or Th.

Whole-rock analysis

REE, Y, Th and U determinations were done by inductively coupled-plasma mass-spectrometry (ICP-MS) after HNO_3 + HF digestion of 0·1000 g of sample powder in a Teflon-lined vessel for 150 min at high temperature and pressure, evaporation to dryness, and subsequent dissolution in 100 ml of 4 vol. % HNO_3. Measurements were carried out in triplicate with a PE Sciex ELAN-5000 spectrometer using Rh and Re as internal standards. Coefficients of variation calculated by dissolution and subsequent analysis of 10 replicates of powdered sample were better than ± 3 rel. % and ± 8 rel. % for analyte concentrations of 50 and 5 p.p.m., respectively.

Textural and modal analysis

Thin sections were studied by optical and scanning electron microscopy (SEM) with back-scattered electron (BSE) and energy dispersive X-ray microanalysis (EDAX). Modal counting was done on selected samples, using four thin sections per sample. The mass fraction of major minerals was calculated by mass balance using average microprobe data of major minerals and whole-rock chemical composition. The modal proportion of REEYThU-rich accessories was estimated with the SEM in two steps, first calculating the overall modal abundance of all bright minerals (REEYThU-accessories, sulphides, Fe–Ti oxides, barite, etc.) by image analyses, and then estimating the relative abundance of each species by identification with EDAX of every bright grain present in the section and recording its apparent diameter. The textural position (inclusion, between two grains, in a triple junction, etc.) and the nature of the surrounding minerals were also recorded. Values of the ratio $\Sigma_1^{i=n} X_i C_i / C_{\text{whole-rock}}$ were between 0·8 and 1·15 for most elements, where X_i is the modal fraction on each phase, and C_i and $C_{\text{whole-rock}}$ are the concentration of a given element in each phase and in the whole rock, respectively.

REE, Y, U and Th analysis of minerals

Major minerals and accessory grains with a grain-size >100 μm were analysed by LA–ICP-MS. Smaller accessory grains were analysed by electron microprobe.

LA–ICP-MS analyses were performed in the Perkin Elmer ICP-MS Applications Laboratory at Überlingen (Germany) with a prototype UV laser ablation system coupled to a high-sensitivity PE Sciex ELAN-6000 ICP-MS spectrometer. The excimer SOPRA Ne:Xe:HCl gas laser was set at

Table 1: Studied geological units

Geological unit	Region	Main features
Differentiated two-mica granites and leucogranite		
Pedrobernardo	Central Iberia	ASI ~ 1·27. Accessory dumortierite
Albuquerque	Central Iberia	ASI ~ 1·25. Cordierite-bearing facies. Accessory andalusite and dumortierite. Related to U ore deposits
Trujillo	Central Iberia	ASI ~ 1·24. Accessory cordierite and tourmaline
Jalama	Central Iberia	ASI ~ 1·24. Sillimanite-bearing facies
Cabeza de Araya	Central Iberia	ASI ~ 1·21. Cordierite- and garnet-bearing facies
Boquerones	Central Iberia	ASI ~ 1·27. Accessory andalusite and cordierite
Ronda leucogranites	SW Iberia	ASI ~ 1·1–1·24. High B contents. Abundant tourmaline and cordierite
Murzinka	Central Urals	ASI ~ 1·1. Accessory garnet in aplites
Uvildy-Ilmen	Central Urals	ASI ~ 1·05–1·13. Accessory garnet
Autochthonous anatectic leucogranites		
Almohalla	Central Iberia	ASI ~ 1·18. Garnet-rich leucogranite, with accessory muscovite and biotite
Tarayuela	Central Iberia	ASI ~ 1·26. Cordierite leucogranite with accessory garnet
Peña Negra	Central Iberia	ASI ~ 1·24. Cordierite leucogranite with accessory biotite
Peraluminous adamellites, granodiorites and tonalites		
Hoyos-Gredos	Central Iberia	ASI ~ 1·24. Biotite–cordierite granodiorites and adamellites
Alberche	Central Iberia	ASI ~ 1·18. Biotite adamellites, with accessory cordierite
Dzyabyk	Central Urals	ASI ~ 1·14. Two-mica adamellites and biotite granodiorites
Cheliabinsk	Central Urals	ASI ~ 1·14. Biotite granodiorites with muscovite-bearing facies
Elanchink	Central Urals	ASI ~ 1·08. Biotite adamellites
Subaluminous granites, granodiorites, tonalites and diorites		
Verkisest	Central Urals	ASI ~ 1·02. Abundant magmatic epidote and titanite. K-poor facies
Shartash	Central Urals	ASI ~ 1·03. Na > K
Shabry	Central Urals	ASI ~ 1·05. Na ~ K
Elanchick	Central Urals	ASI ~ 1·03. Na ⩽ K
Stepninsk	Central Urals	ASI ~ 1·04. K-rich facies
Tagil-Chernoistochinsk	Central Urals	ASI ~ 1·01. Amphibole leucodiorites with no biotite
Khabarny	South Urals	Ophiolitic complex with plagiogranites
Peralkaline granites		
Galiñeiro	N Iberia	Very high REE, Zr, Y, Nb, Th contents. Mineralized facies
Barcarrota	SW Iberia	Riebeckite–aegirine granites
Kelvy	Kola	Riebeckite–aegirine granites
Kharitonovo	Transbaikalia	Riebeckite–aegirine granites
Magnitogorsk	Central Urals	Ferrohastingsite–riebeckite granites
Migmatites		
Peña Negra	Central Iberia	Cordierite–sillimanite–biotite migmatites with occasional accessory garnet
Los Villares	SE Iberia	Cordierite–garnet–sillimanite–biotite
Murmansk block	Kola	Garnet–sillimanite–biotite
Murzinka	Central Urals	Garnet–biotite–sillimanite
Osinovsk	Central Urals	Garnet–biotite–sillimanite–cordierite
Granulites		
Strona	Ivrea–Verbano	Garnet–sillimanite–Kfsp
Murmansk block	Kola	Opx–garnet–kyanite–sillimanite
Ronda	SE Iberia	Garnet–sillimanite–Kfsp
Cabo Ortegal	NW Iberia	Garnet–kyanite–Kfsp

3·8 bars gas pressure. Wavelength was 308 nm, repetition rate 5 Hz, pulse length 30 ns and pulse energy 100 mJ. Data were acquired for 50 s, starting acquisition 10 s after ablation was initiated. The diameter of the laser beam and gas pressure were fixed so as to produce craters with a diameter of ~80 μm in diameter and 40–60 μm in depth, depending on the ablated mineral. Under these conditions, crystals smaller than 100 μm cannot be reliably analysed. Isobaric interferences were automatically corrected by the TotalQuant III© software implemented in the ELAN-6000, which also allows the response factors for all the elements to be adjusted by calibrating the system with an external standard with just a few elements covering the mass range. Calibration was done using the NBS-612 glass, which contains ~40 p.p.m. of most trace elements, as external standard. Concentration values were later refined using silicon as internal standard, previously determined by electron microprobe on the same minerals. In these conditions, detection limits for REE, Y, Th and U were better than 10 p.p.b. Coefficients of variation (CV) obtained by measuring five replicates on a single grain of astrophyllite, which appeared to be unzoned and free of inclusions, were ±4·2 rel. % for 45·6 p.p.m. La, ±18·9 rel. % for 0·57 p.p.m. Y, ±6·4 rel. % for 8·63 p.p.m. U, ±17·5 rel. % for 0·28 p.p.m. Th, ±4·4 rel. % for 4·71 p.p.m. Eu, and ±11·3 rel. % for 0·62 p.p.m. Yb. For elements with concentration higher than 100 p.p.m., CV are normally in the range of ±1–3 rel. %.

Electron microprobe mineral analysis

Major-element, REE, Y, Th and U analyses of minerals were obtained by wavelength dispersive analyses with an ARL electron microprobe operated with PROBE software using as standards the four synthetic glasses described by Drake & Weill (1972)—REE1 Chgo/2, REE2 Chgo/3, REE3 Chgo/4 and REE4 Chgo/5—and the following minerals: Albite Amelia Chgo/18, Mn-Hortonolite Chgo/35, Monazite SPI/32 and Zirconia SPI/47. Accelerating voltage was 20 kV and beam current was 20 nA. Interelemental interferences were suppressed by peak-overlap corrections (Roeder, 1985). Detection limits were better than 0·10–0·05% depending on the element and mineral analysed. Coefficients of variation were close to ±4 rel. % for 1 wt % concentration and ±10 rel. % for 0·25 wt % concentration.

REE, Th AND U COMPOSITION OF MAJOR MINERALS

Micas

REE, Y, Th and U concentrations in micas are very low (Table 2), close to or lower than detection limits (~0·01 p.p.m.) in most cases. Early LA–ICP-MS work on muscovites gave somewhat higher levels (Bea *et al.*, 1994*a*), but it is now recognized that they were probably produced by microinclusions of monazite and xenotime within the ablated spot. Micas from U-rich granites may have several p.p.m. U, especially in hydrothermalized facies, which suggests that uranium is absorbed as uranyl ions, probably in the interlayer position.

Amphiboles and pyroxenes

Orthopyroxenes also have negligible contents of REE, Y, U and Th (Table 3). Amphiboles and clinopyroxenes have appreciable REE and Y, but low Th and U contents (Table 3). Chondrite-normalized REE patterns of Ca-amphibole (Fig. 1) increase progressively from La to Pr and then decrease smoothly from Nd to Lu with no Eu anomaly or a small negative one, more intense in amphiboles coexisting with primary epidote (e.g. analysis 1 in Table 3). Partition coefficients for coexisting Ca-amphibole–Ca-clinopyroxene pairs are $D_{U,Th}^{amp/cpx} \sim 1$ and $D_{REE,Y}^{amp/cpxx} \sim 2$–4. REE patterns of Ca-clinopyroxene are analogous to those of Ca-amphiboles, but at lower concentrations (Fig. 1), and have very small negative or positive Eu anomalies [see also Mazzuchelli *et al.* (1992)].

Na-amphiboles are richer in La–Sm and Tm–Lu than Ca-amphiboles (Table 3). Chondrite-normalized REE patterns decrease uniformly from La to Dy and then increase from Er to Lu, with $Er_N/Lu_N \sim 0·3$–0·6 (Fig. 1). Partition coefficients for Na-amphibole–Na-clinopyroxene pairs are $D_{U,Th}^{Na-amp/Na-cpx} \sim 2$–5, $D_{LREE}^{Na-amp/Na-cpx} \sim 6$–10, $D_{Eu-Er,Y}^{Na-amp/Na-cpx} \sim 4$–6 and $D_{Tm-Lu}^{Na-amp/Na-cpx} \sim 1$–3. REE patterns of Na-clinopyroxene are parallel to those of Na-amphiboles from La to Ho, but the enrichment from Er to Lu is more pronounced (Fig. 1).

K-feldspar and plagioclase

Feldspars have moderate to low LREE contents, and low to very low HREE, Y, Th and U contents (Table 4). Partition coefficients for coexisting plagioclase–K-feldspar pairs are $D_{U,Th,Y}^{plag/Kfsp} \sim 1$, $D_{LREE}^{plag/Kfsp} \sim 1$–5, $D_{Eu}^{plag/Kfsp} \sim 0·3$–3 and $D_{HREE}^{plag/Kfspx} \sim 1$. Chondrite-normalized REE patterns of

Table 2: Selected LA–ICP-MS analyses of primary micas (results are in p.p.m.)

	Biotite						Muscovite					
	1	2	3	4	5	6	1	2	3	4	5	6
Y	0·05	0·25	0·01	0·08	0·09	0·09	0·19	0·01	0·16	0·01	0·06	0·01
U	0·32	0·00	0·00	3·41	0·17	0·01	0·77	0·07	0·16	0·00	0·53	0·21
Th	0·04	0·00	0·10	0·00	0·00	0·21	0·11	0·00	0·03	0·04	0·09	0·00
La	0·11	1·17	0·03	0·03	0·22	0·50	0·34	0·00	0·06	0·04	0·06	0·00
Ce	0·11	0·17	0·00	0·00	0·31	0·50	0·76	0·00	0·15	0·05	0·07	0·02
Pr	0·00	0·11	0·00	0·00	0·02	0·08	0·09	0·04	0·03	0·01	0·03	0·00
Nd	0·00	0·25	0·00	0·00	0·11	0·11	0·00	0·06	0·08	0·04	0·00	0·00
Sm	0·00	0·00	0·00	0·00	0·04	0·04	0·00	0·00	0·03	0·01	0·00	0·00
Eu	0·00	0·04	0·00	0·00	0·11	0·04	0·10	0·00	0·12	0·00	0·00	0·06
Gd	0·00	0·00	0·00	0·00	0·06	0·03	0·03	0·00	0·04	0·02	0·05	0·00
Tb	0·00	0·00	0·00	0·00	0·01	0·00	0·07	0·00	0·00	0·00	0·00	0·00
Dy	0·00	0·00	0·00	0·00	0·05	0·04	0·10	0·00	0·00	0·04	0·00	0·00
Ho	0·00	0·00	0·00	0·00	0·01	0·01	0·03	0·00	0·00	0·01	0·00	0·00
Er	0·00	0·00	0·00	0·00	0·02	0·02	0·11	0·00	0·00	0·02	0·00	0·00
Tm	0·00	0·01	0·00	0·00	0·01	0·00	0·02	0·00	0·00	0·00	0·00	0·00
Yb	0·00	0·00	0·00	0·00	0·01	0·02	0·24	0·00	0·00	0·02	0·00	0·00
Lu	0·00	0·00	0·00	0·00	0·00	0·00	0·00	0·00	0·00	0·00	0·00	0·00
Eu/Eu*	—	—	—	—	6·87	3·53	—	—	10·6	0·00	—	—
La_N/Yb_N	—	—	—	—	14·8	16·8	0·96	—	—	1·35	—	—

Biotites: 1, migmatite (Peña Negra); 2, subaluminous granodiorite (Vierkisest); 3, peraluminous adamellite (Hoyos); 4, U-rich two-mica leucogranite (Albuquerque); 5, subaluminous tonalite (Shabry); 6, peralkaline granite (Magnitogorsk). Muscovites: 1, U-rich two-mica leucogranite (Albuquerque); 2, two-mica granite (Pedrobernardo); 3, peraluminous adamellite (Hoyos); 4, migmatite (Peña Negra); 5, migmatite (Ronda); 6, Be-rich pegmatite (Murzinka).

K-feldspar (Fig. 1) show a variable but always strong LREE–HREE fractionation, usually with intense positive Eu anomaly. REE patterns of plagioclase (Fig. 1) are similar but slightly more enriched in LREE. The intensity of the Eu anomaly in both feldspars is highly variable. Maximum positive anomalies (Eu/Eu* ~25–40) occur in feldspars from migmatites (see analyses 4 in Table 4), whereas the smallest Eu anomalies, even negative ones, appear in feldspars coexisting with magmatic epidote (analyses 5 in Table 4) and in feldspars from extremely differentiated leucocratic segregates from peraluminous granites (Bea *et al.*, 1994*a*). K-feldspars and plagioclases from granulite facies metapelites are remarkably enriched in LREE, with $La_N \geqslant 50$ and $La_N/Sm_N \sim 10$ [e.g. analyses 3 in Table 4; see also ion-probe data of Reid (1990) and Watt & Harley (1993)].

Garnet

Among major minerals, garnet is the richest in Y and HREE (Table 5). The composition of garnet in crustal protoliths shows a marked dependence on whether they come from amphibolite or granulite facies.

Garnets from amphibolite facies are rich in HREE and Y, but have near-zero LREE, Th and U contents [Table 5; see also data of Harris *et al.* (1992)]. Chondrite-normalized REE patterns (Fig. 2) are steeply positive from La to Dy–Er, with $Sm_N/Gd_N < 0{\cdot}6$ and either no Eu anomaly or a small negative one (Eu/Eu* ~0·4–1·4), and then are either flat or decrease smoothly to Lu. Amphibolite-grade garnets are usually zoned, with the HREE and Y either coupled with Mn (Hickmott *et al.*, 1987; Hickmott & Shimizu, 1990) or decoupled from major components (Lanzirotti, 1995; Delima *et al.*, 1995).

Garnets from granulite facies have somewhat lower Y and Dy–Lu, much higher Nd and Sm, higher Sm/Gd ratios ($Sm_N/Gd_N > 0{\cdot}6$), a more pronounced Eu negative anomaly (Eu/Eu* ~0·01–0·2), and a flatter HREE chondrite-normalized pattern than amphibolite-grade garnets [Fig. 2; Table 5; compare also ion-probe data of Reid (1990) and Watt & Harley (1993) with those of Harris *et al.*

Table 3: Selected LA–ICP-MS analyses of amphiboles, clinopyroxenes and orthopyroxenes (results are in p.p.m.)

	Amphibole						Cpx				Opx	
	1	2	3	4	5	6	1	2	3	4	1	2
Y	17·9	19·3	8·69	4·53	9·30	10·2	4·10	2·71	0·37	2·65	0·34	0·28
U	1·76	0·07	0·10	0·14	0·02	0·51	0·18	0·09	0·16	0·13	0·03	0·05
Th	0·25	0·01	0·00	0·00	0·00	0·53	0·00	0·04	0·00	0·10	0·00	0·00
La	8·70	6·85	2·81	1·24	3·82	29·4	1 19	0·20	0·24	3·34	0·03	0·02
Ce	39·4	35·3	12·0	6·72	17·4	83·9	3·16	0·96	0·93	7·43	0·02	0·08
Pr	8·00	7·46	1·93	1·22	2·66	11·8	0·49	0·20	0·18	1·02	0·00	0·01
Nd	39·9	35·1	9·13	6·84	12·5	40·5	2·24	1·29	0·84	4·64	0·00	0·02
Sm	11·5	11·3	2·61	2·01	2·74	9·27	0·74	0·47	0·33	1·16	0·00	0·00
Eu	1·44	3·43	0·88	0·68	0·86	2·77	0·24	0·21	0·10	0·41	0·00	0·00
Gd	9·48	8·47	2·46	1·59	2·43	7·99	0·65	0·56	0·34	1·16	0·00	0·01
Tb	1·53	1·34	0·29	0·23	0·48	1·12	0·10	0·09	0·05	0·18	0·00	0·00
Dy	7·23	7·07	1·25	1·05	2·32	5·13	0·62	0·53	0·32	0·85	0·00	0·00
Ho	1·43	1·37	0·30	0·22	0·51	1·12	0·12	0·11	0·05	0·20	0·00	0·00
Er	3·70	4·11	0·83	0·42	1·36	3·06	0·33	0·27	0·11	0·67	0·00	0·00
Tm	0·51	0·61	0·12	0·06	0·20	0·58	0·05	0·04	0·01	0·24	0·00	0·00
Yb	2·90	3·53	0·78	0·25	1·24	5·00	0·30	0·23	0·08	2·89	0·00	0·00
Lu	0·45	0·54	0·15	0·04	0·20	1·04	0·05	0·03	0·01	0·65	0·00	0·00
Eu/Eu*	0·42	1·07	1·08	1·16	1·02	0·98	1·06	1·25	0·91	1·08	—	—
La_N/Yb_N	2·02	1·31	2·43	3·35	2·08	3·97	2·68	0·59	2·02	0·78	—	—

Amphiboles: 1, granodiorite (Vierkisest); 2, tonalite (Vierkisest); 3, leucodiorite (Chernoistochinsk); 4, tonalite (Shabry); 5, tonalite (Shabry); 6, riebeckite, peralkaline sienite (Kharitonovo). Clinopyroxenes: 1, leucodiorite (Chernoistochinsk); 2, diorite (Chernoistochinsk); 3, gabbro–norite (Khabarny); 4, aegirine, peralkaline granite (Kharitonovo). Orthopyroxenes: 1, granulite (Murmansk); 2, charnockite (Kola).

(1992)]. In some granulitic garnets from Ivrea–Verbano stronalites we also detected significant La and Ce contents (see Fig. 2) with La_N/Sm_N ~0·4–0·8. This feature is discussed below.

Garnets from granites usually have an 'amphibolitic' composition. Some crystals occasionally have a 'granulitic' core, probably relict in origin, surrounded by an 'amphibolitic' rim which seems to be equilibrated with the melt at low pressure [analyses 4c and 4r in Table 5, for example; see also data of Sevigny (1993)].

Cordierite

The contents of REE, Y, Th and U in cordierite range from low or very low to zero (Table 5). Chondrite-normalized REE patterns (Fig. 2) show a moderate decrease from La to Sm, a small negative Eu anomaly and variable Gd–Lu profiles with either a negative or positive slope.

Epidote

Magmatic epidote has high LREE and U contents, and moderate U, HREE and Y contents (Table 6). Primary epidote grains are usually rimmed by a film of secondary LREE carbonates (Fig. 3) such as bastnaesite or parisite, produced by reaction with late- or post-magmatic fluids. This causes the REE concentrations of epidote crystals from the same thin section to vary by a factor of 50. Chondrite-normalized REE patterns (Fig. 4) display a steep decrease from La to Sm, a moderate to strong positive Eu anomaly, and a moderate decrease from Gd to Lu. Remarkably, the partitioning of Eu into epidote is much more intense than into feldspars ($D_{Eu}^{epidote/Kfsp}$ ~20–30; $D_{Eu}^{epidote/plagioclase}$ ~8–20).

Tourmaline

Tourmaline has low REE, Y, Th and U contents (Table 6). Chondrite-normalized REE patterns are

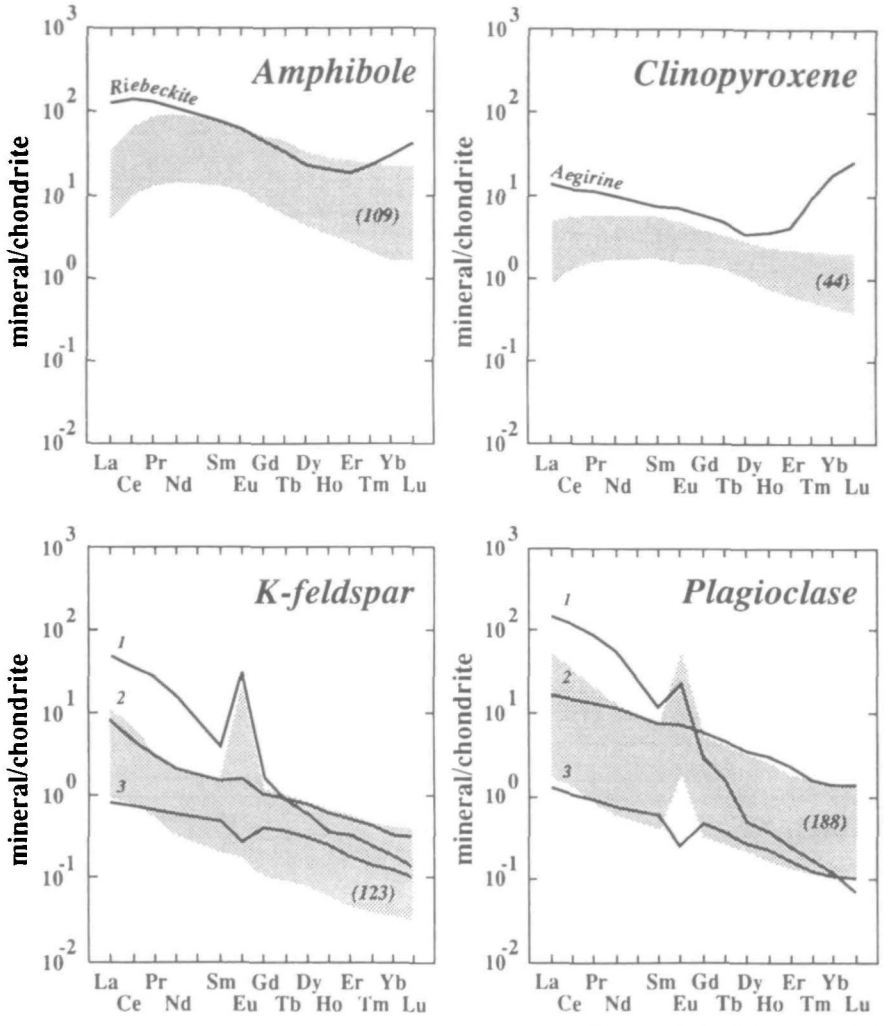

Fig. 1. Chondrite-normalized REE patterns of amphiboles, clinopyroxenes, K-feldspar and plagioclase. Shaded areas represent fields occupied by analysed specimens; the number of analyses represented is shown in parentheses. For K-feldspar and plagioclase, lines 1, 2 and 3 are representative examples of feldspars from a granulite (note the LREE enrichment), feldspars coexisting with primary epidote (note the small positive Eu anomaly) and feldspar from highly fractionated peraluminous rocks (note the low REE contents and negative Eu anomaly), respectively.

so variable (Fig. 2) that at present it is not possible to make any reasonable generalizations.

Al_2O_5 polymorphs

The concentration of REE, Y, Yh and U in all analysed grains of andalusite, sillimanite and kyanite was always lower than the sensitivity of the LA–ICP-MS system.

REEYThU-RICH ACCESSORY MINERALS

We identified about 26 species of REEYThU-rich minerals in common granite rocks and crustal protoliths. Twenty species—monazite, cheralite, xenotime, huttonite, thorite, allanite, cerianite, uraninite, betafite, pyrochlore, brannerite, uranosferite, bastnaesite, parisite, loparite, samarskite, aeschinite, fergusonite, zirkelite and fluocerite—have at least one REE, or Y, or Th, or U as an essential structural component. Six species have at least one of these elements as an occasional abundant impurity: up to a few percent in zircon, up to a few thousand p.p.m. in apatite and sphene, and up to a few hundred p.p.m. in baddeleyite, rutile and fluorite. In the sections below we describe those aspects of the occurrence, composition and textural relationships of REEYThU-rich minerals which are relevant to understanding the geochemistry of these elements in granite rocks. These descriptions only reflect the characteristics of REE-, Th- and U-rich accessories such as they appear in common rocks,

Table 4: Selected LA–ICP-MS analyses of K-feldspar and plagioclase (results are in p.p.m.)

	K-feldspar						Plagioclase					
	1	2	3	4	5	6	1	2	3	4	5	6
Y	0·13	1·25	0·44	0·16	0·40	0·39	0·03	0·08	0·31	0·43	0·65	0·56
U	0·08	10·2	0·37	0·32	0·23	0·37	0·02	0·07	0·23	0·43	0·10	0·42
Th	0·18	0·01	0·10	0·01	0·09	0·08	0·11	0·03	0·11	0·10	0·03	0·09
La	0·19	1·78	10·5	1·39	1·86	0·78	0·64	2·20	34·2	7·33	4·55	1·47
Ce	0·44	2·81	20·8	1·63	2·23	1·71	1·40	3·57	70·8	5·60	9·33	2·62
Pr	0·06	0·28	2·40	0·12	0·28	0·21	0·17	0·40	8·4	0·49	1·19	0·20
Nd	0·27	0·82	6·57	0·29	0·97	0·47	0·50	0·81	25·4	1·38	3·99	0·52
Sm	0·07	0·10	0·59	0·08	0·23	0·08	0·07	0·15	1·77	0·18	1·13	0·12
Eu	0·01	0·66	1·68	0·89	0·09	0·28	0·01	0·23	1·25	1·44	0·29	1·30
Gd	0·08	0·14	0·33	0·08	0·21	0·07	0·07	0·13	0·59	0·15	0·98	0·12
Tb	0·01	0·03	0·03	0·01	0·03	0·01	0·01	0·02	0·08	0·02	0·16	0·02
Dy	0·08	0·13	0·15	0·06	0·19	0·05	0·07	0·09	0·12	0·10	1·01	0·14
Ho	0·01	0·03	0·02	0·01	0·03	0·01	0·01	0·02	0·02	0·02	0·16	0·03
Er	0·03	0·07	0·05	0·02	0·08	0·03	0·04	0·04	0·04	0·06	0·26	0·07
Tm	0·00	0·02	0·01	0·00	0·01	0·00	0·00	0·01	0·00	0·01	0·03	0·01
Yb	0·02	0·07	0·03	0·02	0·05	0·02	0·02	0·03	0·02	0·06	0·12	0·06
Lu	0·00	0·02	0·00	0·00	0·01	0·00	0·01	0·00	0·00	0·01	0·02	0·01
Eu/Eu*	0·41	17·1	11·6	34·0	1·25	13·2	0·44	5·00	3·74	26·8	0·84	33·1
La_N/Yb_N	6·41	17·1	236	46·9	25·1	26·3	21·6	49·4	11·54	82·4	25·5	16·5

1, Aplite (Pedrobernardo); 2, phenocryst in porphyritic U-rich granite (Albuquerque); 3, granulite (Strona); 4, migmatite (Peña Negra); 5, epidote-bearing granite (Vierkisest); 6, tonalite (Shabry).

not in pegmatites, metasomatites, or highly alkaline types.

Minerals with REE, Y, U or Th as essential structural components

Monazite (LREEPO$_4$) and cheralite [ThCa(PO$_4$)$_2$]

Monazite is the most widespread LREE-rich accessory mineral in granitoids, where it appears as isolated minute crystals with a diameter usually smaller than 50–60 μm, which have a great tendency to be included within biotite (Fig. 5), garnet (Fig. 6) and apatite (Fig. 7). Monazite is more abundant in silicic peraluminous types, but may be found in all types of granitoids, regardless of their silica content and degree of alumina saturation. However, when crystallization conditions were extraordinarily favourable for the formation of allanite, such as in granites with magmatic epidote, monazite may be very scarce or absent.

The composition of monazite (Table 7) varies widely owing to substitutions among the rare earths, the effects of solid solution with cheralite [$ThCa(PO_4)_2$] and huttonite ($ThSiO_4$) molecules, and partial replacement of Th by U (e.g. Vlasov, 1966, p. 285; Förster, 1993; Wark & Miller, 1993; Förster & Tischendorf, 1994; Förster & Rhede, 1995). Monazite is a selective mineral for LREE. Chondrite-normalized REE patterns are almost flat from La to Pr and then decrease smoothly from Pr to Yb and Lu, with a strong negative Eu anomaly (Fig. 8). Nd-rich monazites are not uncommon, especially in granulites (analysis 3 in Table 7). Primary monazite has high concentrations of thorium (ThO_2 ~5–27 wt% in unmineralized granites) and moderate concentrations of uranium (UO_2 ~0·2–3 wt%), except in U-rich granites where the situation is reversed (e.g. analysis 2, Table 7). Most thorium is incorporated into the monazite lattice through the cheralitic substitution $Th^{4+} + Ca^{2+} \rightleftharpoons 2LREE^{3+}$; it seems, in fact, that there is a complete solubility between $LREEPO_4$ and $ThCa(PO_4)_2$. The percentage of cheralitic component is usually in the range of 6–18%, but may rise to 50–70% in allanite-rich granites. Single grains of monazite are often zoned, with roughly concentric patterns from a cheralite-rich nucleus to monazite-rich rims predominating. The solubility of $ThSiO_4$ is more limited, usually <5%, even in monazites coexisting with Th-orthosilicate, although it may occasionally

Table 5: Selected LA–ICP-MS analyses of garnets and cordierites from metapelitic rocks and granites (results are in p.p.m.)

	Garnet								Cordierite			
	1	2	3	4	5c	5r	6c	6r	1	2	3	4
Y	157	94·3	58·6	25·9	248	135	45·1	187	0·07	0·55	0·37	0·05
U	0·11	0·21	0·03	0·12	0·08	0·00	0·03	0·18	0·05	0·36	0·16	0·01
Th	0·09	0·10	0·01	0·09	0·00	0·00	0·04	0·07	0·05	0·31	0·19	0·07
La	0·03	0·16	0·97	1·75	0·01	0·04	0·43	0·03	0·08	0·77	0·47	0·11
Ce	0·14	0·17	3·03	4·62	0·04	0·03	0·53	0·00	0·21	1·72	1·09	0·12
Pr	0·05	0·07	0·51	0·61	0·01	0·01	0·07	0·02	0·03	0·20	0·15	0·00
Nd	1·95	1·01	3·13	3·29	0·08	0·14	0·49	0·17	0·12	0·89	0·53	0·00
Sm	6·26	5·37	5·57	5·75	0·06	0·09	2·81	0·32	0·03	0·14	0·15	0·00
Eu	0·01	0·11	0·13	0·11	0·15	0·11	0·21	0 07	0·01	0·05	0·05	0·00
Gd	8·17	8·89	7·69	8·22	5·45	4·69	7·39	3·70	0·05	0·17	0·21	0·00
Tb	1·74	2·03	1·41	2·15	4·20	3·81	2·07	2·34	0·01	0·04	0·04	0·00
Dy	14·7	15·6	10·2	20·2	60·1	44·3	13·1	33·9	0·05	0·30	0·21	0·00
Ho	3·45	4·30	2·23	6·41	21·9	10·8	2·96	14·6	0·01	0·09	0·04	0·00
Er	11·4	15·2	7·13	21·1	75·4	22·0	7·35	68·7	0·03	0·27	0·11	0·00
Tm	1·50	2·63	1·26	3·58	12·5	2·40	1·14	13·6	0·01	0·06	0·01	0·00
Yb	8·93	17·8	8·36	21·5	76·7	11·4	7·10	100	0·04	0·40	0·07	0·00
Lu	1·09	2·43	1·45	3·12	10·2	1·04	1·12	15·3	0·01	0·08	0·01	0·00
Eu/Eu*	0·00	0·05	0·06	0·05	0·80	0·52	0·14	0·20	0·79	0·99	0·86	—
Sm_N/Gd_N	1·01	0·80	0·96	0·92	0·01	0·01	0·03	0·50	0·11			

In the case of garnet, c and r mean core and rim, respectively. Garnet: 1–4, garnet granulites (stronalites, kinzigite formation, Ivrea zone); 5, garnet amphibolite (NW Iberia); 6, granite (Peña Negra). Cordierite: 1, migmatite (Peña Negra); 2, retrograde crystal after garnet (Peña Negra); 3, leucogranite (Peña Negra); 4, leucogranite (Ronda).

reach 30–40% in some (but not all) monazite grains from a given thin section.

We could not find any meaningful correlation between granite typology and the chemistry of monazite. Certainly, monazites from metaluminous granites tend to be rich in cheralitic component and those from Th-rich granites may be rich in huttonitic component, but the compositions of grains from the same thin section usually vary so much [see also Wark & Miller (1993)] that it seems almost impossible to sketch general tendencies.

Secondary monazites appear always hydrated (rabdofan?) and characteristically have very low Th and U contents (analysis 12, Table 7). Most but not all secondary monazites we analysed also have high Y contents.

Allanite

Allanite is, after monazite, the most important LREE carrier in granitoids. Primary allanite may be found in all granite types except in the most peraluminous [aluminium saturation index (ASI) > 1·2] phosphorus-rich varieties, and is especially abundant in granites with magmatic epidote. Contrary to a common belief among petrographers, primary allanite and monazite may coexist in equilibrium (Fig. 9). Secondary allanite is very common, even in the most peraluminous granites (Fig. 7).

Primary allanite usually appears as idiomorphic or subidiomorphic grains, often metamictic, with a diameter ranging from several tens of microns up to a few millimetres. They occur either alone or included within larger crystals, generally epidote or amphibole (Fig. 10).

The chemical composition of allanite is very complex and may vary across a wide range [see Vlasov (1966, pp. 302–306)]. In granites, however, the compositional range of allanite is more restricted [Table 8; see also Petrik *et al.* (1995)]. The ΣREE concentration ranges between 14 and 18 wt % with a clear predominance of LREE and a strong negative Eu anomaly (Fig. 8). Primary allanites always contain some Th (ThO_2 ~0·5–3 wt %), Zr (ZrO_2 ~0–2 wt %) and P (P_2O_5 ~0–0·2 wt %). The concentration of these elements is positively correlated

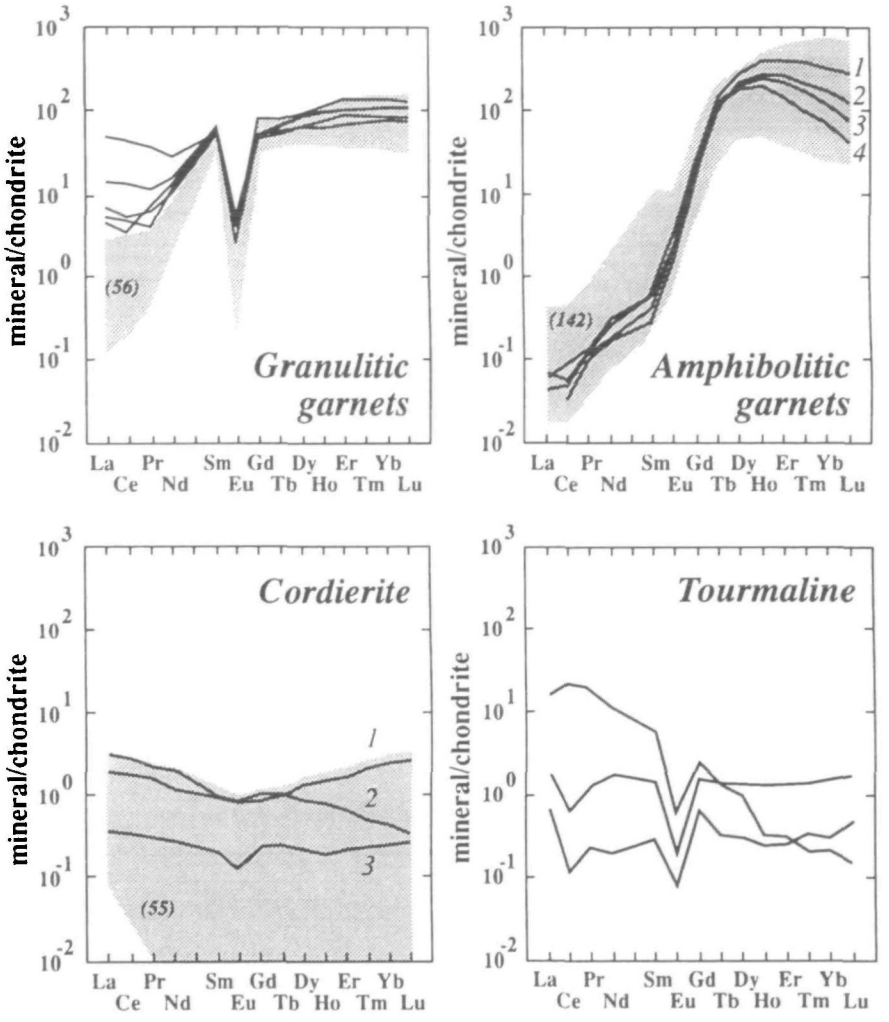

Fig. 2. Chondrite-normalized REE patterns of granulite-grade and amphibolite-grade garnets, cordierite and tourmaline. Shaded areas represent fields occupied by analysed specimens; the number of analyses represented is shown in parentheses. For granulite-grade garnets, continuous lines represent abnormally La–Ce-rich specimens from Ivrea–Verbano stronalites. For cordierites, 1 represents a retrograde crystal after garnet, 2 is an idiomorphic crystal from a granite and 3 comes from a migmatite.

with that of silica (Chesner & Ettlinger, 1989). U and Y contents are usually low and do not show any significant correlation with other elements.

Xenotime [(Y,HREE)PO_4] and intermediate xenotime–zircon phases

Xenotime is isostructural with zircon, coffinite and thorite (Vlasov, 1966, p. 230) and appears to form solid solution series with these minerals, above all with zircon. For convenience and arbitrarily, we have named all members of the xenotime–zircon solid solution series that have ZrO_2 <12 wt% xenotime, all those with P_2O_5 <6 wt% zircon, and all members between these intermediate xenotime–zircon phases (IXZP). As IXZP always occur closely associated with xenotime, they will be described in conjunction with it.

Primary xenotime and IXZP are characteristic of peraluminous leucogranites, but they also occur in peralkaline granites. Both minerals appear either as isolated small grains with a diameter usually smaller than 50 μm or, more often, as complex intergrowths with zircon (Fig. 11).

The theoretical chemical composition of xenotime is YPO_4, but natural specimens in granitoids always contain 5–15 wt% of HREE [Table 9; see also Wark & Miller (1993)]. Besides the $ZrSiO_4$ component, primary xenotime also has ~0·5–2 wt% of LREE, 0·5–2 wt% of UO_2, 0–2 wt% of ThO_2 and appreciable amounts of FeO and CaO. Chondrite-normalized REE patterns (Fig. 8) show a steep increase from La to Sm, a deep negative europium anomaly,

Table 6: Selected LA–ICP-MS analyses of tourmalines and epidotes (results are in p.p.m.)

	Tourmaline						Epidote					
	1	2	3	4	5	6	1	2	3	4	5	6
Y	0·11	0·06	0·07	4·30	1·02	0·01	3·77	6·03	9·56	7·19	3·55	1·81
U	0·24	1·04	0·12	0·00	0·00	0·07	7·53	0·00	0·88	4·29	7·29	1·83
Th	0·20	0·00	0·07	1·56	0·00	0·00	0·37	0·71	0·04	0·60	0·70	0·52
La	0·15	0·25	0·41	0·95	1·24	3·87	53·5	97·1	2·99	20·7	13·0	15·0
Ce	0·07	0·63	0·39	3·21	2·09	13·0	61·3	129·	9·07	48·6	24·3	23·2
Pr	0·02	0·06	0·12	0·68	0·24	1·65	5·26	10·1	1·54	5·90	2·94	2·46
Nd	0·09	0·20	0·75	2·94	0·86	4·80	13·5	21·4	6·19	20·0	12·5	7·14
Sm	0·04	0·00	0·23	0·94	0·13	0·82	2·23	2·71	1·64	3·74	1·96	0·91
Eu	0·01	0·00	0·01	0·08	0·00	0·04	2·70	5·40	0·69	2·75	0·88	1·06
Gd	0·13	0·00	0·32	1·62	0·26	0·49	1·56	1·51	1·13	3·26	1·93	0·67
Tb	0·01	0·00	0·05	0·25	0·04	0·05	0·20	0·23	0·18	0·46	0·24	0·09
Dy	0·07	0·00	0·26	1·52	0·32	0·22	0·91	1·37	0·98	2·53	1·54	0·63
Ho	0·01	0·00	0·07	0·32	0·07	0·02	0·20	0·26	0·20	0·51	0·30	0·14
Er	0·04	0·00	0·18	0·91	0·23	0·05	0·51	0·69	0·46	1·31	0·72	0·37
Tm	0·01	0·00	0·03	0·16	0·04	0·01	0·06	0·10	0·06	0·22	0·10	0·06
Yb	0·04	0·00	0·21	0·85	0·26	0·03	0·41	0·58	0·36	1·37	0·54	0·28
Lu	0·01	0·00	0·07	0·14	0·05	0·00	0·06	0·09	0·05	0·20	0·09	0·04
Eu/Eu*	0·42	—	0·11	0·20	0·00	0·19	4·43	8·17	1·55	2·41	1·38	4·15
La_N/Yb_N	2·53	—	1·32	0·75	3·22	87·0	88·1	113	5·61	10·2	16·2	36·1

Tourmaline: 1 and 4 leucogranites (Ronda); 2, U-rich granite (Albuquerque); 3 and 5, migmatites (Peña Negra); 6, granite (Trujillo). Epidote: 1–3, granodiorites (Vierkisest); 4, granite (Vierkisest); 5 and 6, granodiorites (Shartash).

and then another increase from Gd to Yb and Lu, not as abrupt as before. In some rare cases, LREE rise to 3 wt% and produce REE patterns which appear as if some monazitic component could also be dissolved in xenotime (Fig. 8). Additional support for this idea comes from the fact that Th increases together with LREE.

Intermediate xenotime–zircon phases have lower REE contents than pure xenotime, and the predominance of HREE over LREE is also less pronounced (Fig. 8). In addition, they are richer in Al_2O_3, FeO and CaO, which increase with the zircon component.

Thorium orthosilicate ($ThSiO_4$) minerals: huttonite and thorite

Very low but still significant amounts of thorium orthosilicate minerals—the monoclinic huttonite and the tetragonal thorite—are scattered through all types of granitoids. They appear as minute grains included in major (Fig. 12) and accessory minerals, above all zircon (Fig. 13) [see also Rubin *et al.* (1989)]. Because the huttonite and thorite can be differentiated with SEM only by the morphology of the sections, we could not establish the relative proportion of these two minerals, although the fact that $ThSiO_4$ minerals in metaluminous granites are often metamictic, whereas in peraluminous granites they appear remarkably unaltered, could perhaps indicate that they consist of thorite and huttonite, respectively (Bayer, 1969).

$ThSiO_4$ minerals from granites always contain several weight percent of REE (Table 10), with a strong predominance of HREE over LREE and deep negative Eu anomalies (Fig. 8). Some P-rich varieties having high concentrations of LREE are probably intermediate monazite–huttonite phases (analysis 3, Table 10). Uranium is usually in the range of 1–10 wt%, although grains with subequal contents of Th and U (uranothorite?) are frequent.

Uraninite (UO_2)

Uraninite is a common accessory in peraluminous leucogranites, where it appears as very small grains (diameter usually <5 μm) included either in major or accessory minerals, especially zircon (Fig. 14). Uraninite contains up to 20 wt% ThO_2 and may also have up to 5 wt% of Y_2O_3 and 1 wt% of REE,

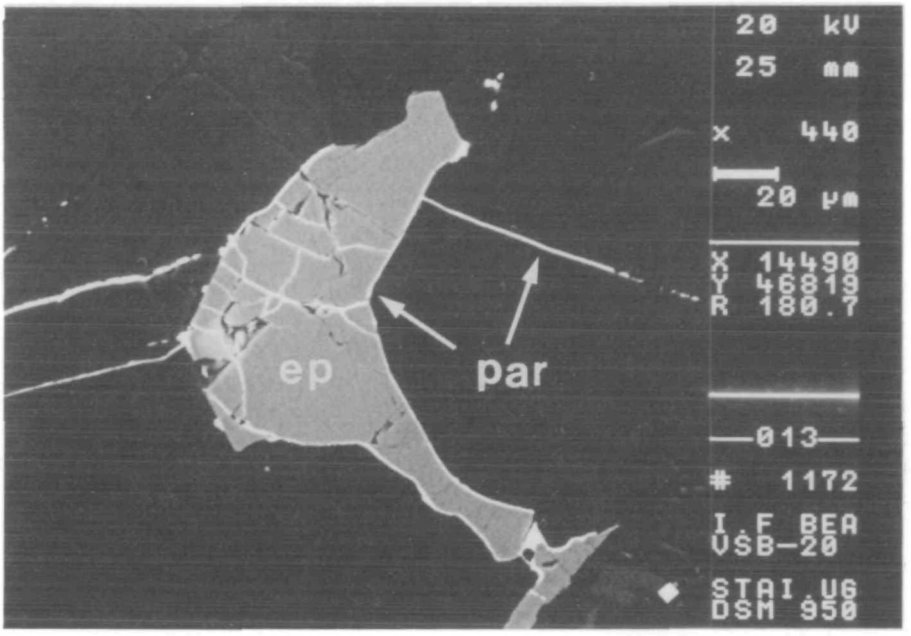

Fig. 3. Back-scattered electron (BSE) SEM image of a primary epidote crystal rimmed by REE-carbonate (parisite?). (Note how REE-carbonate fills radiating cracks.) Metaluminous granodiorite, Verkisest batholith.

with a clear predominance of HREE (Table 10; Fig. 15).

Complex uranium minerals

Rocks containing uraninite and xenotime usually contain other primary U minerals as well. The most common species are minerals from the pyrochlore–betafite [$(U,Ca)(Nb,Ta,Ti)_3O_9.nH_2O$] group. A U–Bi mineral, probably uranosferite [$BiUO_3(OH)_2$] and brannerite (UTi_2O_6) are also occasionally found. All these minerals contain variable amounts of Th and REE, and are generally HREE selective (Table 10; Fig. 15).

Aeschinite, samarskite, fergusonite, loparite

Complex minerals of Nb, Ti, Y, U and REE are common in peralkaline granitoids, usually forming complex aggregates of phases with a highly variable composition (Montero, 1995) (Table 10; Fig. 15). The most abundant species are aeschinite (low U and Y, high LREE), fergusonite (moderate U, Y and LREE, high HREE) and samarskite (high U, Y and HREE, low LREE). Loparite is one of the richest minerals in La–Ce (see analysis 11, Table 10) although it appears to be limited to highly peralkaline rocks.

Bastnaesite and parisite

Primary bastnaesite is found only in REE-rich peralkaline granitoids. Secondary REE carbonates, probably parisite and/or bastnaesite, are fairly common in metaluminous granites, where they appear as a product of the decomposition of allanite and epidote (Figs 3 and 10). These minerals are extremely selective for LREE and contain negligible amounts of Th and U.

Cerianite (CeO_2)

The oxide of tetravalent Ce is found in some hydrothermalized granites filling cracks and veins. As cerianite is usually related to monazites with a deep negative Ce anomaly (Fig. 8; analysis 1 in Table 7), it would seem to be produced through the oxidation and subsequent leaching of Ce^{4+} from monazite caused by hydrothermal fluids. The concentration of Y, Th, U and REE other than Ce in cerianite is below microprobe sensitivity.

Zirkelite [$(Zr,Ca,Ti,Fe,Mg,REE,U,Th)_3O_5$]

Zirkelite is a rare mineral which appears in low-silica granitoids together with thorite and baddeleyite, usually as very small inclusions in zircon (Fig. 13). Its rarity and small grain-size have not permitted us to obtain reliable analyses, although semi-quantitative EDAX analyses with SEM indicate UO_2 ~3–7 wt %, and the predominance of HREE over LREE, with Dy_2O_3 ~0·5 wt %, Er_2O_3 ~ 0·7 wt % and Yb_2O_3 ~0·9 wt %.

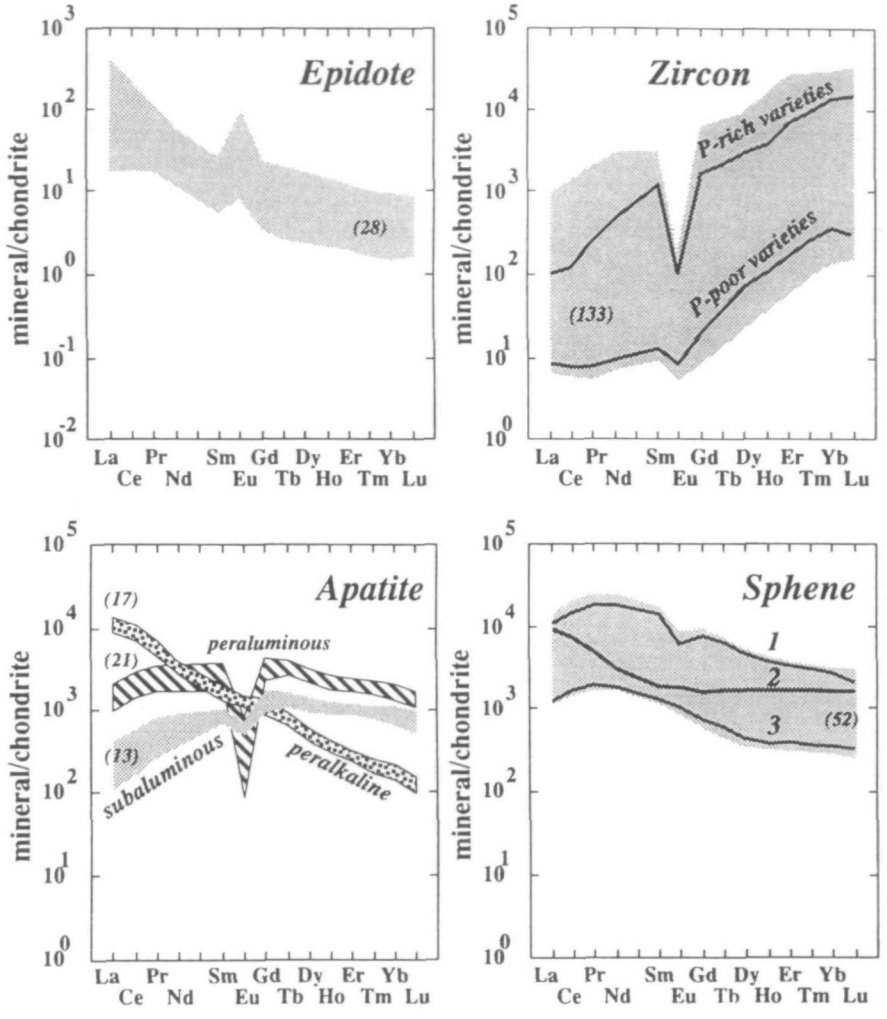

Fig. 4. Chondrite-normalized REE patterns of epidote, zircon, apatite and sphene. Shaded areas represent fields occupied by analysed specimens; the number of analyses represented is shown in parentheses. For sphene, 1 and 3 represent extreme cases of sphenes from metaluminous granitoids (note the decreased intensity of the Eu anomaly as ΣREE decreases; 2 represents the characteristic pattern of sphenes from peralkaline granites.

Fluocerite [$(La,Ce)_3F$]

Fluocerite is an occasional mineral in peralkaline granitoids (Imaoka & Nakashima, 1994; Montero, 1995), where it normally appears as a late mineral growing in interstitial positions. It contains about 18–20 wt % La, 33–35 wt % Ce, 1·5–2 wt % Pr, 6–6·5 wt % Nd, 0·4–0·5 wt % Sm, 0·4–0·6 wt % Gd and <0·1 wt % of the other REE. Th content may be as high as 2 wt %. U and Y are usually very low.

Minerals with REE, Y, Th or U as abundant impurities

Zircon ($ZrSiO_4$)

Zircon is the most ubiquitous accessory mineral in granitoids, having been extensively studied owing to its many applications in isotopic dating and as a petrogenetic indicator (Pupin, 1980; Krasnobayev, 1986; Aleinikoff & Stoeser, 1989; Heaman & Parrish, 1991). Zircon appears as grains with ϕ_{max} usually between 60 and 1 μm, which frequently contain micron-sized inclusions of thorite (Fig. 13) and uraninite (Fig. 14), and may form complex intergrowths with xenotime (Fig. 11) and, less commonly, with monazite (Fig. 16).

The chemical composition of zircon varies within a broad range owing to replacement of Zr^{4+} by Hf^{4+}, Th^{4+} and U^{4+}, as well as to solid solution with xenotime, which introduces elevated amounts of Y and HREE in the zircon lattice [Table 11; see also Heaman *et al.* (1990), Pupin (1992), Rub *et al.* (1994) and Barbey *et al.* (1995)]. The concentrations of Th and U are highly variable, even among grains from the same thin section. ThO_2 is rarely greater

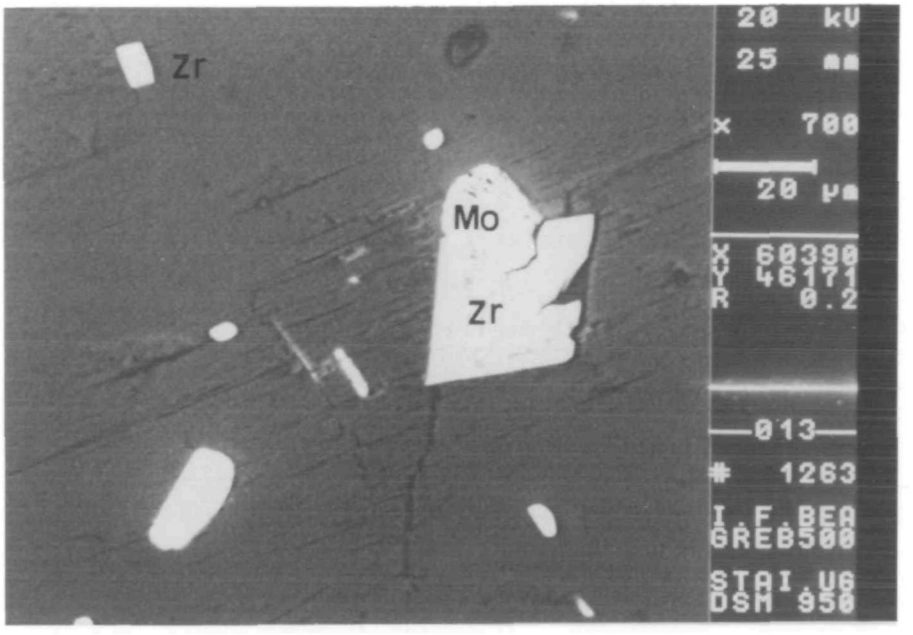

Fig. 5. BSE-SEM image of a biotite crystal from a peraluminous granite. [Note the great abundance and small grain-size of zircon (Zr) and monazite (Mo and unlabelled) inclusions.] Pedrobernardo granite.

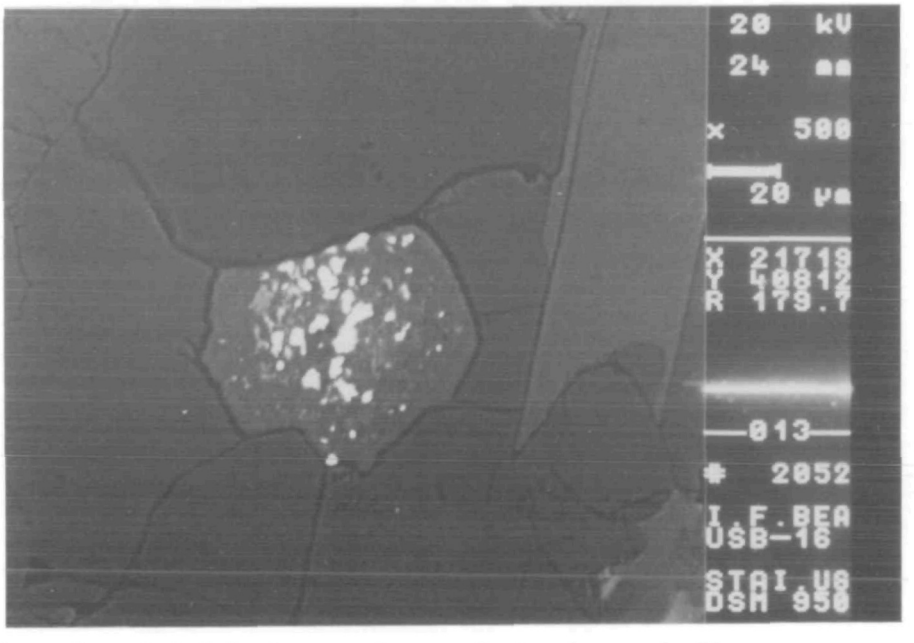

Fig. 6. BSE-SEM image of monazite inclusions in a garnet from a peraluminous leucogranite. (Note how monazite is selectively included in garnet.) Murzinka granite.

than 0·75 wt %, and LA–ICP-MS data show that values between 100 and 200 p.p.m. are common (Table 11). UO_2 may occasionally reach 10 wt %, but normal concentrations are between 10 and 100 p.p.m. U (Table 7). The concentration of Y varies from a few p.p.m. to 6 wt %, and increases with increasing phosphorus contents (Tourrette *et al.*, 1991). ΣHREE are in the range of 0–2 wt % and also increase with phosphorus, which suggests that solid solution with xenotime is the main mechanism of Y and REE incorporation into the zircon lattice. Chondrite-normalized REE patterns (Fig. 4) show La_N/Sm_N in the range 1–5, a moderate negative Eu anomaly and a progressive increase in HREE, with

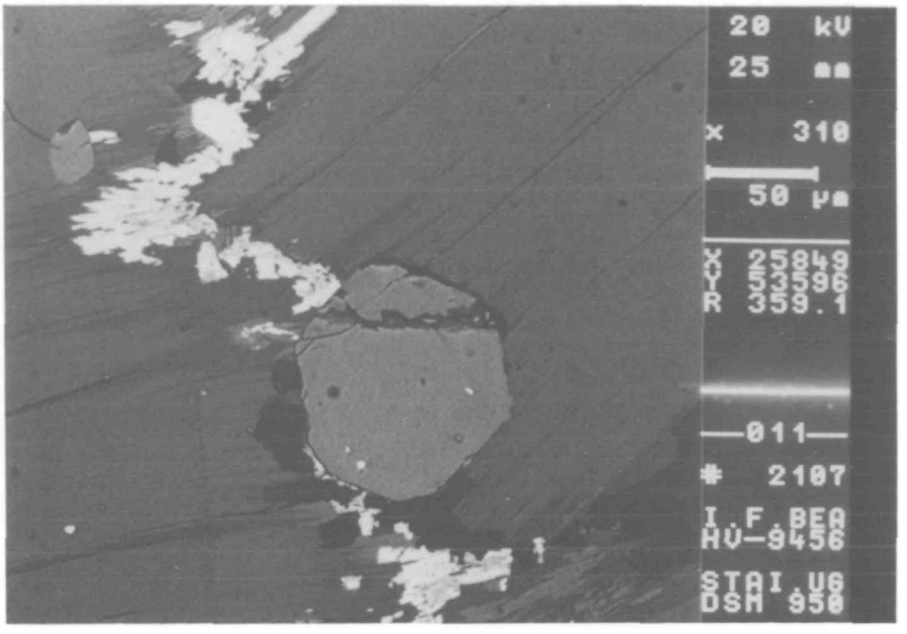

Fig. 7. BSE-SEM image of secondary allanite that developed along a fracture in biotite. The pseudohexagonal large crystal is apatite. White small grains included in apatite and biotite are monazite. Hoyos granodiorite.

Gd_N/Yb_N ~5–10 and occasionally $Yb_N/Lu_N > 1$. Sc is a common trace element with a concentration in zircons from granites rarely higher than some tens of p.p.m. (Heaman *et al.*, 1990), although we have found one case (Albuquerque granite, Iberia) with zircons having up to 10 wt% Sc_2O_3 (analysis 11, Table 11).

Apatite [$Ca_5(PO_4)_3(OH,F,Cl)$]

Apatite is a well-known abundant accessory mineral in granite rocks, especially in peraluminous granodiorites and monzogranites, where it may reach 1% modal abundance. Apatite appears in grains of variable size and morphology, from small (~30–5 µm), needle-like crystals, more characteristic of I- and A-type granites, to large (~500–50 µm), roughly equidimensional crystals typical of strongly peraluminous S-type granites. Apatite crystals usually contain small inclusions of monazite (Fig. 7).

The concentration of REE, Y, Th and U in apatite is highly variable (Roeder *et al.*, 1987) and shows marked differences according to the rock's aluminosity (Table 12; Fig. 4). Apatites from peraluminous rocks are the richest in Y, U, Th and HREE, and have flat chondrite-normalized REE patterns (La_N/Lu_N ~1) with a strong negative Eu anomaly (Eu/Eu* ~0·1). Apatites from metaluminous granites have less REE, Y, Th and U, and their REE patterns show a positive slope from La to Sm, a small negative Eu anomaly (Eu/Eu* ~0·7), and are almost flat from Gd to Lu, with La_N/Lu_N ~0·1–0·4 (Fig. 4). Apatites from peralkaline rocks have the lowest Y, REE, Th and U contents, but are the richest in LREE, have no Eu anomaly, and show REE patterns with a steep negative slope from La to Lu (La_N/Lu_N ~50–100).

Sphene [$CaTi(SiO_4)(O,OH,F)$]

Primary sphene is a widespread accessory in metaluminous and peralkaline granites, where it usually appears as idiomorphic or subidiomorphic crystals with a grain-size in the range of 0·05–5 mm. Primary sphenes always contain a few thousand p.p.m. REE and Y, and a few hundred p.p.m. Th (Table 13). The concentration of U, however, is highly variable, from near zero to ~500 p.p.m. Chondrite-normalized REE patterns of sphene (Fig. 4) from metaluminous granites increase from La to Pr–Nd, have a small negative Eu anomaly (less intense the less REE the crystal has), decrease from Gd to Dy–Ho, and are almost flat from Er to Lu. Sphenes from peralkaline rocks, in contrast, have REE patterns with a negative slope from La to Sm, no Eu anomaly, and are almost flat from Gd to Lu.

Baddeleyite, fluorite and rutile

These minerals have been reported to contain somewhat elevated concentrations of REE, Y, Th and/or U (Vlasov, 1966; Heaman & Parrish, 1991).

Table 7: Selected microprobe analyses of monazite crystals (results expressed in percent)

	1	2	3	4	5	6	7	8	9	10	11	12
SiO_2	0·00	0·00	4·74	2·50	0·40	0·00	0·00	0·08	0·00	0·00	0·00	0·92
ZrO_2	0·01	0·15	0·00	0·17	0·16	0·05	0·30	0·00	0·26	0·28	0·10	0·34
Al_2O_3	0·00	0·99	0·00	0·00	0·00	0·05	0·00	0·00	0·00	0·00	0·15	0·62
FeO	0·00	0·30	0·01	0·00	0·00	0·63	0·21	0·00	0·05	0·00	0·79	0·15
MgO	0·00	0·00	0·00	0·00	0·00	0·00	0·00	0·00	0·00	0·00	0·00	0·00
CaO	2·79	2·15	0·41	1·28	1·02	1·58	2·88	2·11	2·11	1·48	1·18	1·75
Na_2O	0·00	0·02	0·00	0·00	0·00	0·00	0·05	0·00	0·00	0·00	0·00	0·11
P_2O_5	34·05	28·96	21·07	23·51	30·04	30·62	28·22	24·80	28·70	28·42	28·51	25·65
Y_2O_3	2·88	2·86	0·96	2·93	3·62	1·61	2·36	3·25	0·04	2·22	0·33	7·67
ThO_2	10·58	4·78	27·31	18·64	8·54	9·22	9·98	10·01	11·75	8·94	5·42	0·00
UO_2	0·18	13·78	0·81	1·46	1·58	1·18	6·47	1·35	0·90	0·79	1·14	0·48
La_2O_3	13·62	7·83	6·43	9·18	8·29	10·27	8·15	8·77	9·31	11·37	6·49	6·36
Ce_2O_3	2·42	21·01	18·88	23·34	25·79	26·47	24·03	25·26	27·20	28·15	29·36	20·92
Pr_2O_3	5·50	2·84	2·81	3·72	3·74	3·07	3·57	3·65	3·97	4·20	3·22	2·73
Nd_2O_3	18·34	9·76	13·59	8·51	11·20	11·48	10·46	14·99	12·63	10·17	16·80	9·58
Sm_2O_3	2·15	2·63	1·15	2·21	3·70	2·55	2·27	3·58	2·07	2·59	3·04	1·87
Eu_2O_3	0·14	0·22	0·18	0·24	0·14	0·08	0·05	0·07	0·15	0·24	0·19	0·01
Gd_2O_3	0·59	0·66	0·49	1·40	0·89	0·83	0·39	1·67	1·12	0·58	1·82	2·11
Dy_2O_3	0·27	0·42	0·46	0·64	0·59	0·37	0·15	0·91	0·38	0·13	0·31	2·42
Er_2O_3	0·06	0·02	0·18	0·07	0·08	0·15	0·08	0·16	0·14	0·07	0·15	0·77
Yb_2O_3	0·03	0·01	0·15	0·09	0·03	0·11	0·07	0·03	0·12	0·07	0·12	0·72
Lu_2O_3	0·00	0·00	0·03	0·01	0·00	0·02	0·01	0·00	0·01	0·01	0·02	0·20
Total	93·61*	99·39	99·66	99·90	99·81	100·34	99·68	100·69	100·91	99·71	99·14	85·38*

* Contains appreciable H_2O.

1, Cerianite-bearing granite (Ilmen); 2, U-rich peraluminous leucogranite (Albuquerque); 3, metapelitic granulite (Strona); 4, garnet leucogranite (Murzinka); 5, B-rich leucogranite (Ronda); 6, two-mica granite (Pedrobernardo); 7 and 8, allanite-bearing granite (Magnitogorsk); 9, allanite-bearing granodiorite (Sirostan); 10, xenotime-bearing peraluminous leucogranite (Ronda); 11, xenotime-bearing migmatite (Peña Negra); 12, secondary monazite (Galiñeiro).

However, in all the samples we studied these elements are below microprobe sensitivity. On the other hand, the small grain-size has not allowed us to perform reliable LA–ICP-MS analyses. Some laser shots at crystals slightly smaller than the laser beam—and therefore with some contribution from the surrounding crystals—indicate that these three minerals are LREE selective and the concentrations of REE and Y are lower than a few tens of p.p.m. Analysis of a baddeleyite concentrate from Kovdor (Kola) also shows a minor enrichment in HREE, producing a U-shaped REE pattern, very similar to that described by Reischmann *et al.* (1995) in baddeleyite concentrates from South Africa. The U and Th concentrations are probably a few p.p.m., except in rutile, where U is probably in the range of 20–100 p.p.m.

FRACTIONAL CONTRIBUTION OF EACH MINERAL TO WHOLE-ROCK REE, Y, Th AND U CONCENTRATIONS

The nature and, in some cases, the composition of REEYThU-rich accessories changes systematically with the rock bulk-chemistry, above all with aluminosity. Therefore, to obtain a general picture of the fractional contribution of major and accessory minerals to the bulk-rock REE budget for the whole granite spectrum, we performed a mass-balance study of 12 plutons from Iberia and the Urals with an average ASI ranging from 1·27 to 0·78. The following features stand out.

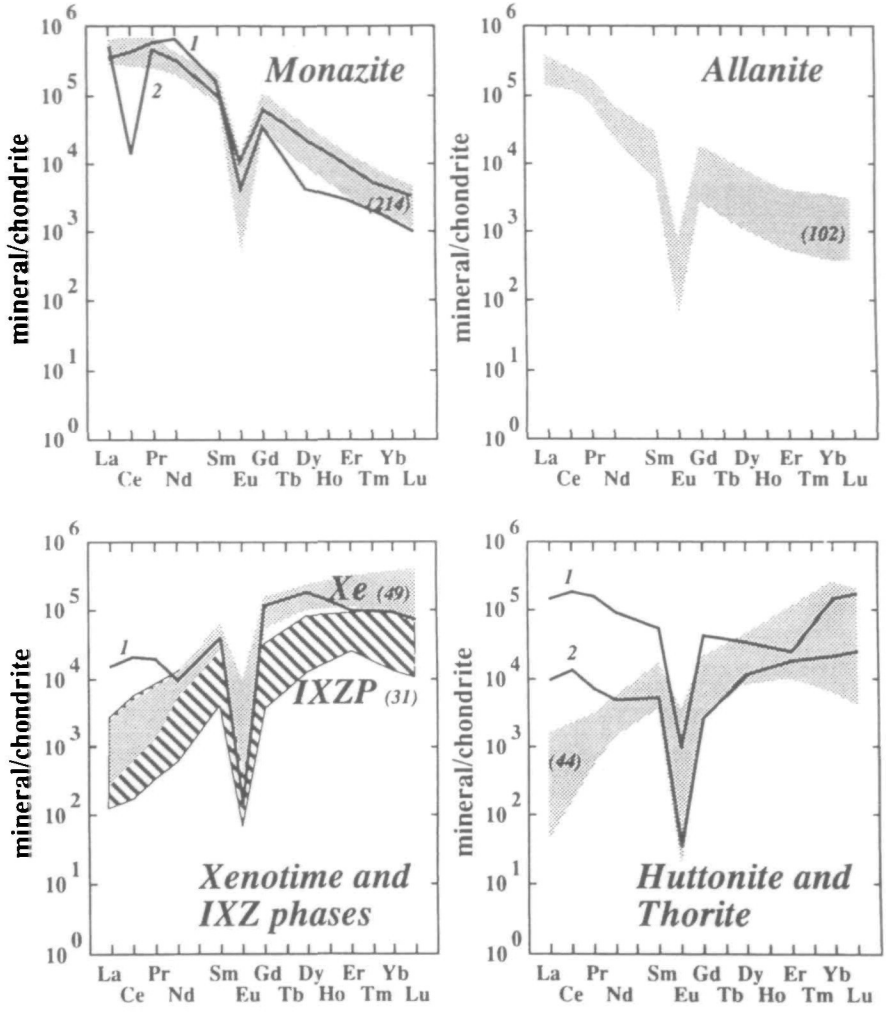

Fig. 8. Chondrite-normalized REE patterns of monazite, allanite, xenotime, intermediate xenotime–zircon phases (IXZP) and Th-orthosilicate minerals. Shaded areas represent fields occupied by analysed specimens; the number of analyses represented is shown in parentheses. Monazite: 1, Nd-rich variety; 2, Ce-depleted monazite associated with secondary cerianite (see text). Xenotime: 1, intermediate xenotime–monazite phase. Th-orthosilicates: 1 and 2, LREE- and P-rich varieties, probably monazite–huttonite solid solution phases.

Distribution of LREE (Fig. 17)

In peraluminous granites, ~90–95 wt % of bulk-rock LREE contents reside within accessories (80–85 wt % in monazite, the rest in apatite) and the remaining 5–10 wt % in feldspars. In metaluminous granites, the fraction of LREE residing within accessories decreases to ~70 wt % (50–60 wt % in allanite, the rest in sphene, apatite, monazite and REE-carbonates). Amphibole accounts for ~15–25 wt % LREE, whereas the remaining 5–10 wt % is in feldspars and, when present, epidote. In peralkaline granites, the fraction of LREE residing within accessories increases again up to 80–90 wt %. Allanite is still a substantial LREE reservoir, although bastnaesite, fluocerite and aeschinite may also be very important.

Distribution of Eu (Fig. 17)

In peraluminous granites, plagioclase and K-feldspar contain similar fractions of total Eu, and together they account for ~90 wt % Eu. Apatite plus monazite accounts for ~5–7 wt % Eu and micas could have ~1–2 wt % Eu. In metaluminous granites, plagioclase is the most important Eu reservoir and together with K-feldspar accounts for ~70–80 wt % of total Eu. Amphibole may account for ~5–15 wt % and the rest is in allanite, sphene, apatite and monazite. When present, primary epidote may also account for a significant fraction of total Eu. In peralkaline granites, ~75 wt % Eu is in feldspars, another 10 wt % in alkali amphiboles, and the rest is distributed in allanite, epidote, sphene, monazite, bastnaesite, niobotantalates, etc.

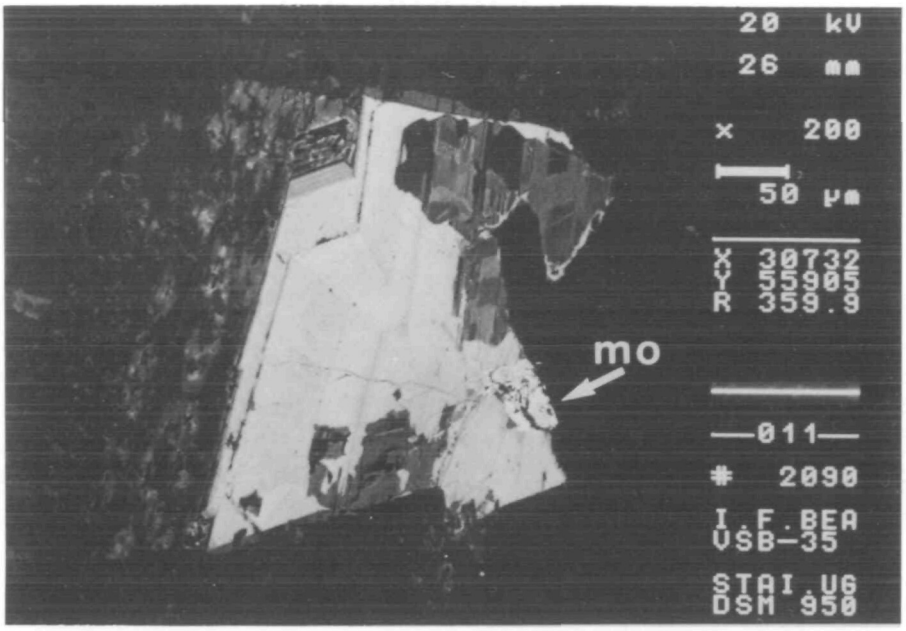

Fig. 9. BSE-SEM image of an idiomorphic-zoned allanite including a cheralitic monazite crystal, apparently in equilibrium (see text). Metaluminous plagiogranite, Ackermanovsky complex, Khabarny.

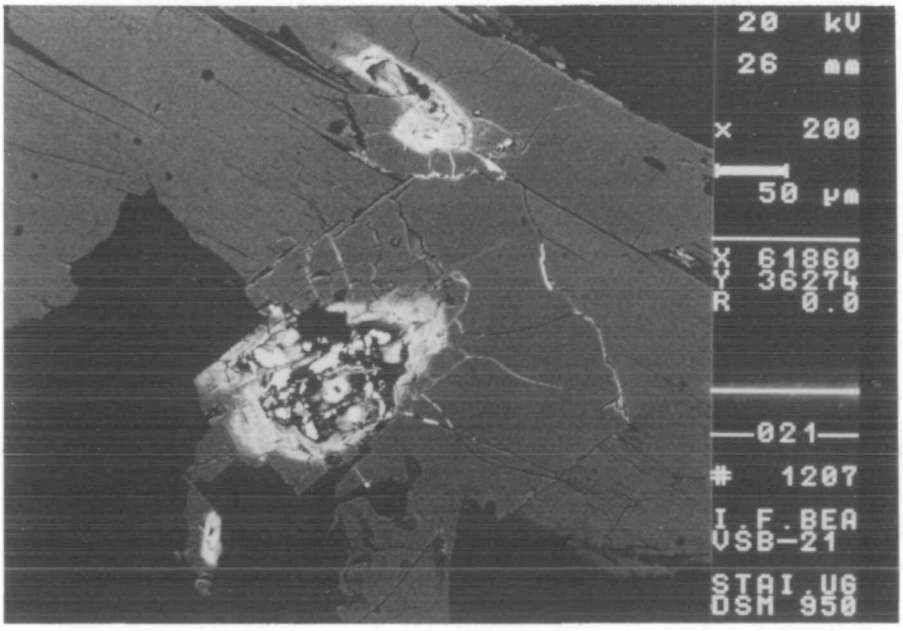

Fig. 10. Metamictic allanite crystals included in amphibole. [Note secondary REE-carbonates filling cracks (BSE-SEM image).]

Distribution of HREE and Y (Fig. 17)

In peraluminous granites, no less than 95 wt % of total HREE reside within accessories. In low-Ca varieties, the fraction of total REE that resides within xenotime is ~30–50 wt %, in apatite ~15–25 wt %, in zircon ~15–20 wt %, in monazite ~5–10 wt %, and in Th-orthosilicate ~5–10 wt %. The disappearance of xenotime in high-Ca peraluminous granites reinforces the roles of zircon (~35–40 wt % of total HREE), monazite (~20 wt %) and apatite (20–25 wt %). In metaluminous granites, amphibole may contain as much as 30–35 wt % of total HREE, whereas zircon accounts for ~30–50 wt %, allanite

Table 8: Selected analyses of allanite crystals (results expressed in percent)

	1	2	3	4	5	6	7	8	9	10	11
SiO_2	32·95	37·28	34·15	30·14	36·43	38·21	42·66	42·35	33·43	32·10	31·88
ZrO_2	0·06	0·08	0·02	0 00	0·28	0·76	1·64	1·45	0·07	0·13	0·00
Al_2O_3	14·86	12·14	16·16	14·02	15·67	16·04	13·56	13·36	11·01	10·74	13·68
FeO	18·22	17·53	17·50	17·07	10·87	10·83	9·09	8·91	16·23	17·07	13·51
MgO	1·20	0·02	0·75	0·24	1·03	1·00	0·67	0·84	0·10	0·01	1·22
CaO	10·39	9·31	9·86	9·09	10·95	10·15	9·87	9·34	8·37	8·78	10·14
Na_2O	0·12	0·08	0·14	0·22	0·19	0·23	0·56	0·50	0·19	0·22	0·06
P_2O_5	0·08	0·02	0·04	0·03	0·04	0·16	0·12	0·14	0·00	0·01	0·09
Y_2O_3	0·34	0·22	0·37	0·19	0·52	0·24	0·365	0·229	0·147	0·236	0·271
ThO_2	0·72	0·64	0·56	0·66	1·31	1·67	1·79	2·05	1·05	1·31	0·96
UO_2	0·00	0·00	0·00	0·00	0·00	0·00	0·22	0·011	4·38	0·101	0·093
La_2O_3	4·47	5·06	4·75	8·94	4·84	4·87	4·87	3·97	5·72	4·630	4·67
Ce_2O_3	9·50	9·82	8·97	14·13	10·01	9·76	8·53	8·79	12·27	14·73	13·96
Pr_2O_3	1·28	1·32	1·18	1·65	1·21	1·25	0·90	1·28	1·40	1·71	1·51
Nd_2O_3	2·68	2·74	2·45	0·48	3·16	2·17	1·30	1·88	4·07	4·82	5·06
Sm_2O_3	0·43	0·43	0·43	0·08	0·47	0·36	0·27	0·269	0·230	0·300	0·640
Eu_2O_3	0·00	0·00	0·00	0·00	0·00	0·00	0·00	0·001	0·001	0·003	0·001
Gd_2O_3	0·25	0·36	0·09	0·07	0·37	0·17	0·14	0·159	0·130	0·174	0·430
Tb_2O_3	n.d.	n.d.	n.d.	n.d.	n.d.	n.d.	n.d.	0·021	0·016	0·023	0·055
Dy_2O_3	0·19	0·23	0·03	0·07	0·10	0·06	0·11	0·101	0·085	0·130	0·210
Ho_2O_3	n.d.	n.d.	n.d.	n.d.	n.d.	n.d.	n.d.	0·020	0·014	0·020	0·033
Er_2O_3	0·07	0·07	0·01	0·03	0·04	0·01	0·05	0·048	0·036	0·053	0·073
Tm_2O_3	n.d.	n.d.	n.d.	n.d.	n.d.	n.d.	n.d.	0·006	0·004	0·006	0·008
Yb_2O_3	0·05	0·06	0·01	0·02	0·03	0·01	0·03	0·031	0·020	0·030	0·032
Lu_2O_3	0·00	0·01	0·00	0·00	0·00	0·00	0·00	0·004	0·003	0·003	0·004
Total	97·86	97·42	97·47	97·11	97·52	97·95	96·75	95·76	98·97	97·34	98·59

*Contains appreciable H_2O.
REE, Y, Th and U were determined by LA–ICP-MS in samples 8–11. All the other data were obtained by electron microprobe. 1, 2 and 10, granodiorite (Vierkisest); 3 and 4, granite (Magnitogorsk); 5 and 11, plagiogranite (Khabarny); 6, leucogranite (Shartash); 7, 8 and 9, tonalite (Sirostan). n.d., not determined.

for ~5–15 wt %, sphene for ~5–10 wt %, Th-orthosilicate for ~2–5 wt %, and apatite plus monazite for the remaining 5–10 wt %. In peralkaline granites, the fraction of HREE in major minerals decreases down to 5 wt %. Niobotantalates contain ~40–60 wt % HREE, xenotime has ~20–30 wt %, and the rest is in zircon and thorite. Yttrium shows basically the same distribution pattern as HREE.

Distribution of Th (Fig. 18)

In peraluminous granites, the fraction of Th residing within major minerals is very low, ~5 wt %. Monazite, with ~65–80 wt %, and Th-orthosilicate, with ~20–30 wt %, are the most important Th reservoirs, whereas zircon, xenotime and apatite account for ~1–2 wt % each. In metaluminous granites, amphibole contains ~15–20 wt % of total Th, feldspars ~5 wt %, allanite ~10–40 wt %, monazite ~15–70 wt %, Th-orthosilicate ~10–25 wt %, sphene and zircon ~2–10 wt %, and the rest is in apatite. In peralkaline granites, the fraction of Th contained in major minerals decreases down to 5–15 wt %, whereas the roles of Th-orthosilicate (~20–40 wt %) and niobotantalates (~1–10 wt %) increase. Monazite contains ~20–40 wt % Th, allanite ~5–20 wt %, sphene ~5 wt %, and the rest is in zircon and apatite.

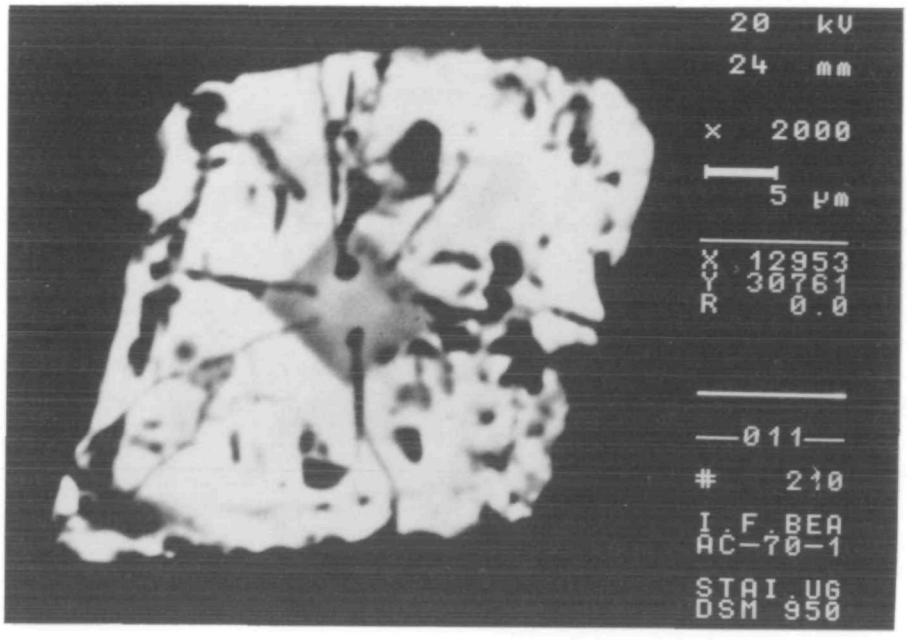

Fig. 11. BSE-SEM image of a xenotime–zircon intergrowth. The idiomorphic nucleus has an external part composed of zircon and a core comprising IXZP. The external part is mostly composed of xenotime, with alternating thin layers of IXZP. Ronda leucogranites.

Distribution of U (Fig. 18)

The fraction of U contained in major minerals is always <5 wt %. In low-Ca peraluminous granites, U resides mostly in xenotime (~50–60 wt %), followed by uraninite, monazite ~5–20 wt %, betafite–pyrochlore and zircon. In high-Ca peraluminous granites, zircon and xenotime contain ~85–90 wt % of total U, whereas Th-orthosilicate and uraninite account for 5–10 wt % U. In metaluminous granites, zircon accounts for 50–60 wt % U, allanite for 10–20 wt % U, apatite plus xenotime for 15–30 wt % and Th-orthosilicates for 5–10 wt % U. In peralkaline granites, niobotantalates, especially samarskite, may become the most important U reservoirs.

DISCUSSION

Effects of accessories on the geochemistry of REE, Y, Th and U

Effects derived from the high fraction of REE, Y, Th and U contained in accessories

The fractionation of minute amounts of accessories will dramatically influence the partitioning of REE, Y, Th and U between melt and solids, simply because accessories contain most of these elements. This study on the contribution of major and accessory minerals, despite the unavoidable analytical inaccuracies and the arbitrariness of sample selection, unequivocally confirms that major minerals play a very subordinate role with respect to that of accessories (Gromet & Silver, 1983), especially in peraluminous systems. At the same time, as REE, Y, Th and U are essential structural components in at least one accessory phase of every crystallizing granite and melting protolith, they do not generally obey Henry's law during melt–solid partitioning, their concentrations in partial melts not being ruled by crystal–melt distribution coefficients but by solubility relations and dissolution kinetics (Rapp & Watson, 1986). These latter, in their turn, depend strongly on the volatile content and bulk-composition of the system (Watt & Harley, 1993).

Effects of textural position during partial melting

The textural position and small grain-size of REEYThU-rich accessories further complicates the partitioning of REE, Y, Th and U during melt segregation. The behaviour of accessory minerals during partial melting depends on whether they are placed at major-phase grain boundaries or are included within major minerals (Watson *et al.*, 1989). In the first case, accessories are available for the melt and so react with it. In the second case, accessories may remain physically isolated from the melt, thus preventing any reaction, or may be entrained as inclusions if major minerals are incorporated into the melt as restitic crystals (Watt & Harley, 1993; Bea *et al.*, 1994*b*). Based on facial energy considerations and experimentation, Watson

Table 9: Selected microprobe analyses of xenotime and intermediate xenotime–zircon (IXZ) crystals (results expressed in percent)

	1	2	3	4	5	6	7	8	9	10	11	12
SiO_2	1·11	0·31	0·22	0·31	0·75	1·02	1·00	3·20	8·37	16·00	9·65	11·52
ZrO_2	0·00	0·11	0·13	0·16	0·24	0·29	0·41	4·95	11·08	23·91	28·29	38·45
HfO_2	0·03	0·12	0·05	0·00	0·00	0·00	0·00	0·02	0·32	1·05	0·28	0·93
Al_2O_3	0·00	0·00	0·00	0·00	0·00	0·00	0·00	0·78	0·66	3·86	2·17	2·00
FeO	0·26	0·13	0·36	0·61	0·00	0·10	0·00	2·31	0·30	3·16	1·59	1·35
MgO	0·00	0·00	0·00	0·04	0·00	0·00	0·00	0·02	0·01	0·11	0·03	0·07
CaO	0·10	0·14	0·11	0·12	0·15	0·98	0·13	0·80	0·29	0·90	1·64	1·61
Na_2O	0·00	0·05	0·01	0·00	0·02	0·05	0·00	0·08	0·09	0·32	0·05	0·06
P_2O_5	31·84	33·01	33·34	32·88	31·85	29·02	30·75	25·18	25·90	20·87	23·31	19·28
Y_2O_3	46·91	50·07	48·97	44·82	47·17	44·84	47·20	45·51	36·50	4·86	22·36	15·30
ThO_2	0·85	0·18	0·12	0·17	0·59	0·00	1·15	1·73	1·62	16·77	0·00	0·15
UO_2	1·90	0·00	0·00	0·00	2·27	9·44	2·02	1·94	0·59	1·25	2·10	1·81
La_2O_3	0·02	0·03	0·03	0·01	0·03	0·02	0·06	0·04	0·42	0·07	0·07	0·00
Ce_2O_3	0·14	0·15	0·16	0·13	0·16	0·07	0·17	0·26	1·55	0·80	0·11	0·03
Pr_2O_3	0·05	0·04	0·03	0·00	0·05	0·01	0·04	0·05	0·21	0·12	0·04	0·01
Nd_2O_3	0·42	0·38	0·36	0·43	0·39	0·36	0·56	0·43	0·54	0·61	0·35	0·19
Sm_2O_3	0·63	0·63	0·56	0·65	1·08	0·68	0·95	0·86	0·68	0·29	0·42	0·39
Eu_2O_3	0·06	0·00	0·00	0·00	0·00	0·00	0·00	0·00	0·00	0·00	0·00	0·00
Gd_2O_3	1·86	1·91	1·84	1·60	3·33	1·94	2·84	2·34	2·61	0·53	0·83	0·63
Dy_2O_3	4·53	5·31	5·11	4·49	6·42	5·31	5·64	5·27	5·16	0·95	2·38	1·88
Er_2O_3	4·41	4·32	4·61	5·23	2·95	3·04	3·26	2·74	1·84	0·55	2·00	1·33
Yb_2O_3	4·30	2·71	3·96	6·32	2·36	2·78	1·74	1·75	1·65	0·30	2·01	1·57
Lu_2O_3	0·65	0·29	0·61	1·04	0·30	0·55	0·18	0·20	0·21	0·03	0·38	0·24
Total	100·07	99·89	100·58	99·01	100·11	100·50	98·10	100·46	100·60	97·35	100·06	98·80

1, Peraluminous granodiorite (Hoyos); 2, migmatite leucosome (Peña Negra); 3, cordierite leucogranite (Boquerones); 4, two-mica granite (Pedrobernardo); 5: B-rich leucogranite (Ronda); 6, U-rich leucogranite (Albuquerque); 7, peraluminous leucogranite (Trujillo); 8 and 9, leucogranite (Murzinka); 10–12, IXZ from Albuquerque leucogranites.

et al. (1989) concluded that, although included accessories are common in anatexites and high-grade metamorphic rocks, larger accessories representing a significant mass fraction tend to be located at major-phase grain boundaries and must therefore be involved in crustal melting. Our observations on peraluminous migmatites and high-grade gneisses from Iberia agree with that idea but emphasize the role of grain-size. Certainly, in the case of apatite grains—almost equidimensional, with a diameter between 1000 and 10 μm—the mass fraction located at major-mineral boundaries is ~80 wt%, in excellent agreement with Watson *et al.* (1989). However, this is not the situation for monazite, xenotime and zircon, because their grain-size is significantly smaller, usually <30 μm. Results of modal counting with SEM repeatedly indicate that the mass fraction of monazite, xenotime and zircon located at major-phase grain boundaries is <20 wt%, whereas >70 wt% of the mass of these minerals is included within biotite, which thus physically controls the behaviour of REE, Y, Th and U during melt segregation.

Effects of grain-size during fractional crystallization

The vertical distribution of crystals in a convecting magma chamber may be estimated using Bartlett's equation [1969, equation (24)]:

$$\ln Np_2/Np_1 = \left[\frac{(\delta_c - \delta)g}{18\eta K}\left(\frac{1700vK^{1/3}}{\alpha_T g(T_1 - T_2)}\right)\right]d_c^2 \quad (1)$$

where Np_2 and Np_1 are the mineral particle popu-

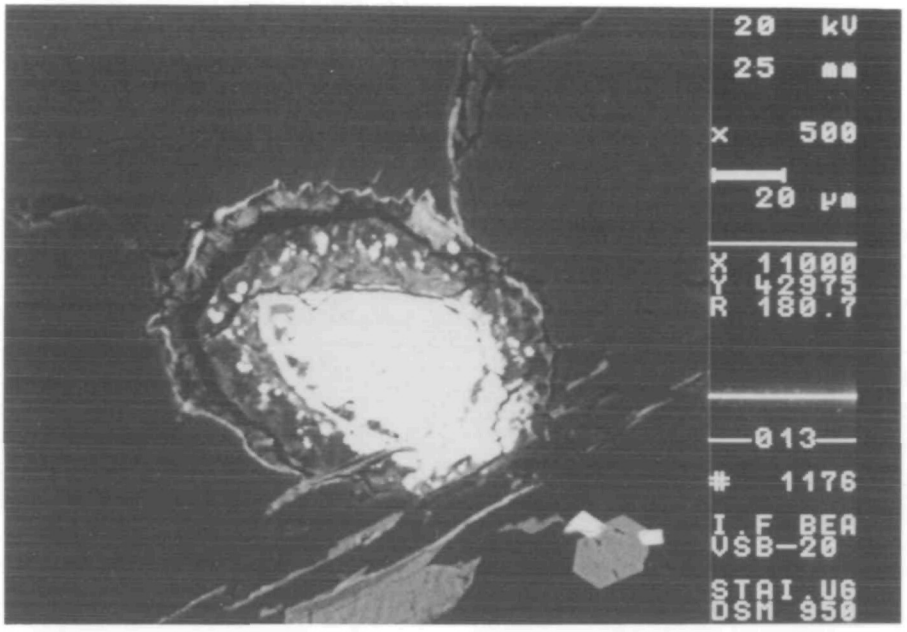

Fig. 12. BSE-SEM image of a radiation-damage structure around a metamictic Th-orthosilicate grain, probably thorite, included in amphibole. The small pseudo-hexagonal grain in the lower right part is an apatite half-including two zircon grains. Sirostan tonalites.

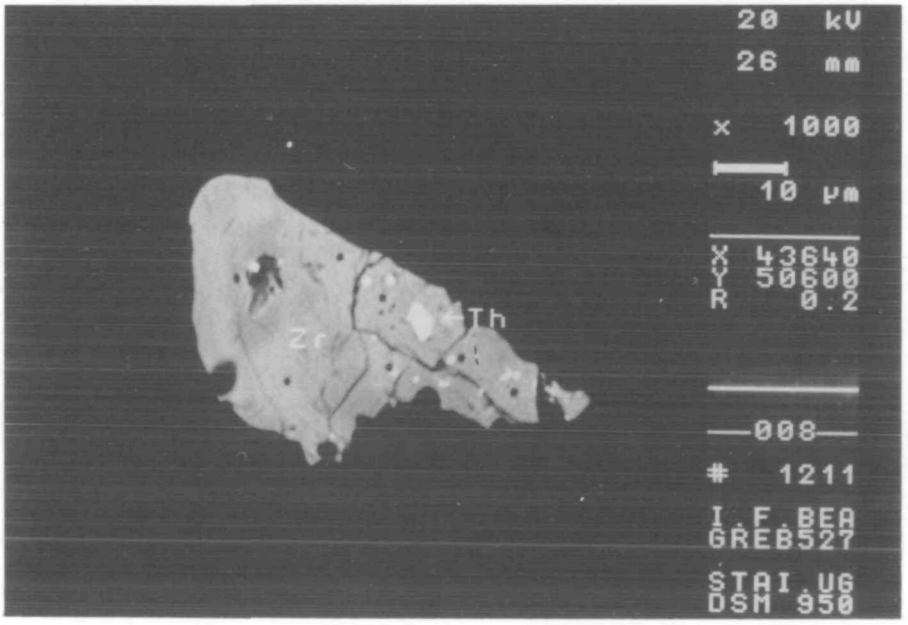

Fig. 13. BSE-SEM image of a xenomorphic zircon grain with microinclusions of Th-orthosilicate, baddeleyite and zirkelite. Burguillos del Cerro diorite.

lation densities in the magma near the ceiling and the floor, respectively; δ_c and δ are the densities of crystal and melt, respectively; g is the gravity acceleration; K is the magma thermal diffusivity; η is the magma viscosity; ν is the kinematic viscosity; T_1-T_2 represents the temperature difference between floor and ceiling; α_T is the thermal expansion coefficient; and d_c is the crystal diameter.

Figure 19 shows settling curves as a function of the diameter of settling minerals, calculated from equation (1) for crystallizing granite melts with a density of 2·5 g/cm^3, viscosity from 10^5 to 10^8 poises,

Table 10: Selected microprobe analyses of other REEYThU-rich accessories (results expressed in percent)

	1	2	3	4	5	6	7	8	9	10	11
SiO_2	13·26	17·56	12·60	0·28	0·58	2·14	0·10	0·39	0·14	0·61	0·00
ZrO_2	0·10	0·00	0·12	0·01	0·01	0·25	0·31	0·71	0·81	0·89	0·00
Nb_2O_5	0·41	0·31	0·05	0·66	0·48	54·21	29·22	4·90	24·59	25·60	12·28
Ta_2O_5	0·05	0·03	0·00	0·21	0·17	3·17	7·61	0·31	0·82	1·07	0·19
$FeO^{tot.}$	1·93	7·53	1·24	0·97	2·35	2·61	4·39	3·90	7·13	8·54	0·02
TiO_2	0·00	0·03	0·00	0·00	0·06	9·18	17·07	17·41	3·59	5·79	30·51
CaO	1·48	0·56	4·51	0·00	0·01	3·99	4·29	5·63	5·48	1·39	2·37
Na_2O	0·02	0·14	0·05	0·03	0·04	0·00	0·21	0·19	1·99	0·05	7·14
P_2O_5	3·05	0·55	10·07	0·21	0·63	0·13	0·08	0·01	0·01	0·04	0·00
Y_2O_3	0·84	3·14	3·57	0·18	0·49	3·5	0·52	2·35	8·34	12·97	0·10
ThO_2	76·44	55·56	38·78	17·51	11·22	2·14	5·69	2·59	3·14	2·98	0·58
UO_2	1·46	7·37	1·11	78·93	83·36	7·28	22·80	2·41	5·76	13·33	0·06
La_2O_3	0·02	0·00	3·99	0·00	0·01	0·06	0·12	12·33	2·19	0·50	17·08
Ce_2O_3	0·06	0·01	12·70	0·01	0·03	0·14	0·24	22·43	6·48	0·90	24·39
Pr_2O_3	0·02	0·01	1·65	0·00	0·01	0·02	0·03	3·08	1·33	0·41	1·58
Nd_2O_3	0·10	0·07	4·82	0·03	0·04	0·06	0·12	11·90	6·44	3·08	2·57
Sm_2O_3	0·09	0·11	0·90	0·08	0·08	0·03	0·03	2·62	3·07	2·46	0·10
Eu_2O_3	0·00	0·01	0·01	0·00	0·01	0·00	0·00	0·25	0·39	0·30	0·01
Gd_2O_3	0·15	0·10	0·93	0·11	0·14	0·06	0·03	2·41	4·16	4·29	0·04
Dy_2O_3	0·21	0·49	0·96	0·16	0·19	0·16	0·04	2·53	7·19	7·74	0·00
Er_2O_3	0·16	1·00	0·45	0·13	0·17	0·21	0·04	1·25	4·46	5·08	0·00
Yb_2O_3	0·11	4·63	0·40	0·09	0·14	0·34	0·07	0·55	2·08	2·57	0·00
Lu_2O_3	0·01	0·61	0·07	0·00	0·04	0·06	0·01	0·05	0·19	0·23	0·00
Total	99·97	99·82	98·98	99·60	100·26	89·74	93·02	100·20	99·78	100·82	99·02

Th-orthosilicates: 1, peraluminous granodiorite (Hoyos); 2, peralkaline granite (Galiñeiro); 3, phosphothorite, peralkaline granite (Galiñeiro). Uraninite: 4, cordierite-bearing granodiorite (Gredos); 5, U-rich leucogranite (Albuquerque). Pyrochlore: 6, peralkaline granite (Keivy). Betafite: 7, peraluminous granodiorite (Hoyos). Aeschynite: 8, peralkaline granite (Kharitonovo). Fergusonite: 9, peralkaline granite (Galiñeiro). Samarskite: 10, peralkaline granite (Galiñeiro). Loparite: 11, peralkaline syenite (Kola).

mineral densities from 4 to 6 g/cm^3 and T_1-T_2 of 50°C. As the dependence of T_1-T_2 is rather weak (Bartlett, 1969), the above parameter set will represent the situation in most crystallizing granites. Figure 19 also shows a curve representing the relative mass fraction of REEYThU-rich accessories as a function of grain-size calculated by averaging modal counting on granites mentioned in Fig. 17. It is evident that even grains of 150 μm with a density as high as 6 g/cm^3 cannot settle appreciably within a melt with a viscosity as low as 10^5 poises. Unmodified uraninite crystals may have a density of 10·3 g/cm^3, but their diameter is usually so small that gravity settling is also impossible. We therefore conclude that the fate of early crystallized REEYThU-rich accessories is to remain in suspension within the melt until a crystallizing major mineral includes them.

The reasons why accessories are selectively included within a few major minerals are not well understood yet, but must surely be diverse. In rocks crystallized from a melt, heterogeneous nucleation—either of the major mineral on an early-crystallized accessory or vice versa—coupled with crystallization related to local saturation adjacent to a growing phenocryst (Bacon, 1989) seem to be the most probable mechanisms. In metasedimentary rocks, detritic inheritance and the neoformation of accessories in some preferential places during sedimentation and diagenesis, complicated later by recrystallization during metamorphism, are the key factors. It is clear in both cases, however, that

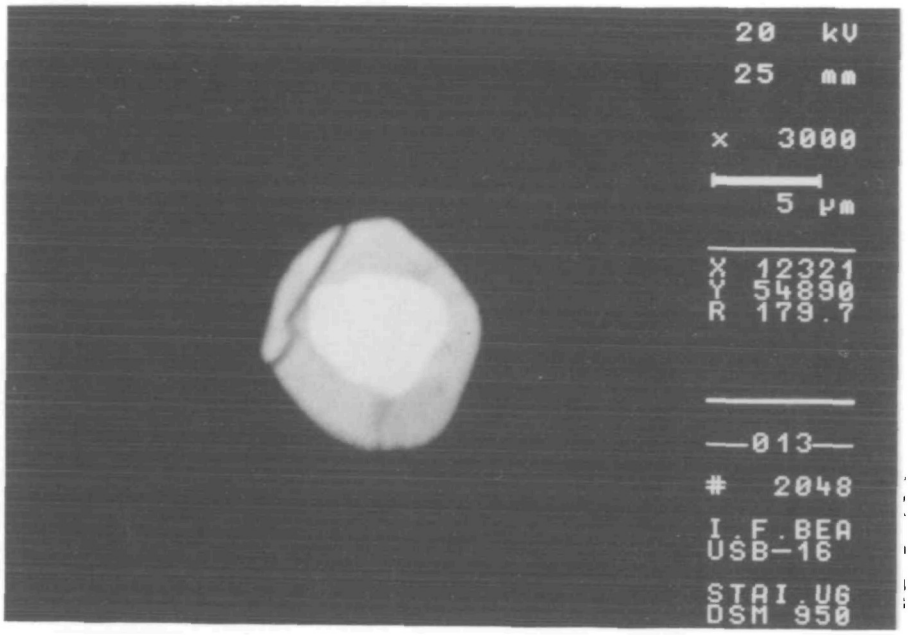

Fig. 14. Zircon growing on a uraninite crystal (BSE-SEM image). Murzinka granite, the Urals.

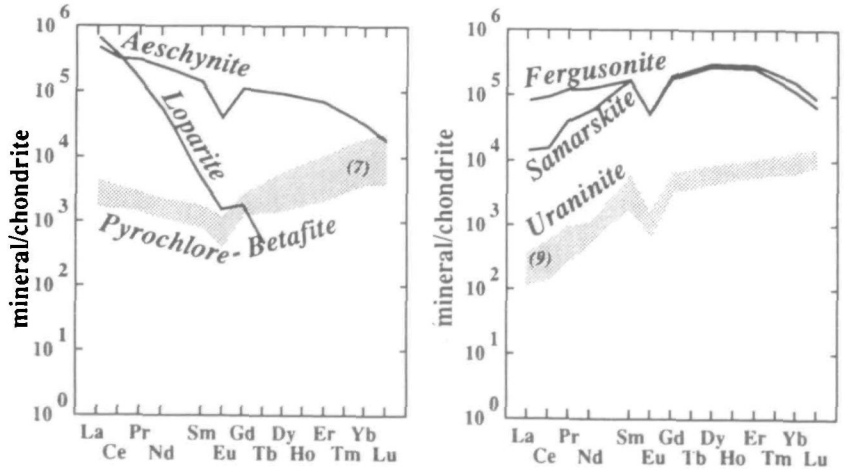

Fig. 15. Chondrite-normalized REE patterns of REEYThU-rich niobotantalates, uraninite and pyrochlore–betafite minerals.

selective inclusion of REEYThU-rich accessories in a given major mineral confers on it an indirect but still significant control over the geochemistry of REE, Y, Th and U, which is almost impossible to quantitatively model with present knowledge.

Contrasting geochemistry of REE, Y, Th and U in subaluminous vs peraluminous granites

The geochemical behaviour of REE, Y, Th and U in differentiated granites changes with aluminium saturation. In general, the higher the aluminium saturation index [ASI = mol. $Al_2O_3/(CaO + Na_2O + K_2O)$], the stronger the depletion in REE (except Eu), Y, Th and U in leucocratic differentiates (Bea, 1993). A good example, which may have important consequences for the understanding of heat production in the crust, is the contrasting vertical distribution of REE, Y, Th and U (and K) in vertically zoned plutons: in I-type granitoids the concentrations of REE, Y, Th and U increase from the least to the most differentiated facies, accumulating upwards (Sawka & Chappell, 1988), whereas in S-type granitoids, in contrast, the concentrations of REE, Y, Th and U decrease from the least to the most differentiated facies, accumulating downwards (Bea *et al.*, 1994*a*). These differences are due to variations in the nature of the major and accessory

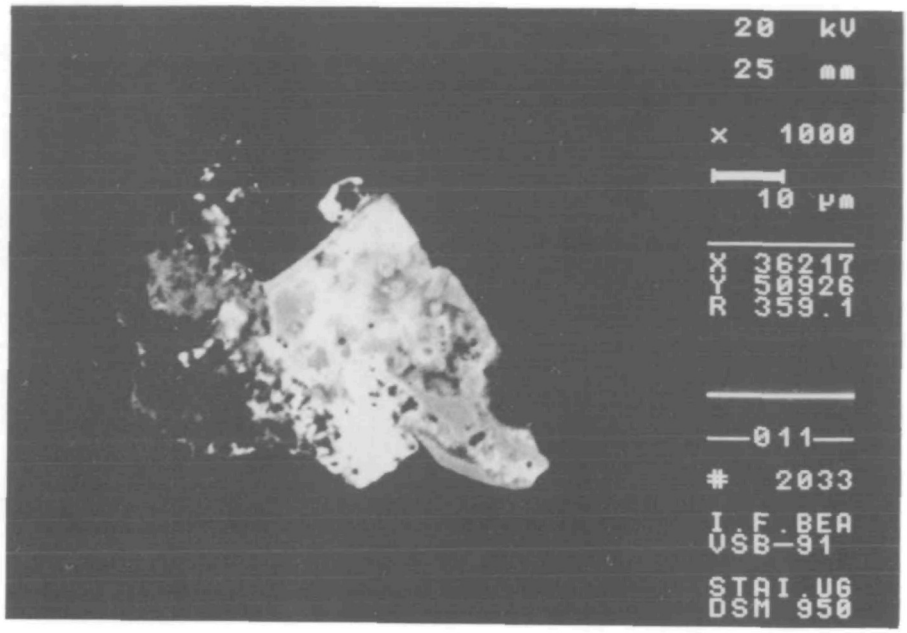

Fig. 16. BSE-SEM image of a complex monazite (white)–zircon (grey) intergrowth.

minerals as a consequence of changes in the aluminium saturation, the key factor being the progressive replacement of allanite and sphene by monazite and xenotime with increasing ASI and decreasing CaO, which seems to occur in the following way.

Peraluminous granites have higher phosphorus contents than metaluminous granites with the same silica content, owing to the enhancement of apatite solubility at high ASI values (London, 1992; Bea *et al.*, 1992; Pichavant *et al.*, 1992; Wolf & London, 1994). As the solubility of monazite and xenotime remains very low regardless of aluminosity (Rapp & Watson, 1986; Wolf & London, 1995), phosphorus-rich peraluminous melts become saturated in monazite and xenotime at low REE concentrations. Precipitated REE-phosphates are then effectively removed from the melt as inclusions in biotite, also an early crystallized mineral, thus producing a strong depletion of REE, Y, Th and U in residual melts. In metaluminous melts, however, the scarcity of phosphate anions makes the saturation in REE-phosphates occur at higher REE concentrations than in peraluminous melts, and allanite and sphene become the dominant REEYThU-carriers. As these minerals are by far less effective than monazite and xenotime at removing these elements from the melt, and they do not usually precipitate massively at the beginning of crystallization, bulk crystal–melt distribution coefficients should remain at $D^{crystal/melt}_{REE,Y,Th,U} < 1$ during most of the crystallization history, thus producing somewhat enriched differentiates.

Post-magmatic mobility of REE, Y, Th and U

REE, Y, Th and U are highly mobile during post-magmatic stages. SEM images revealed that (1) primary epidote is usually rimmed by a film of LREE carbonates which also fill cracks radiating from the epidote grain (Fig. 3), (2) primary allanite is also the source of secondary migrating LREE carbonates (Fig. 10), and (3) secondary allanite forms easily from monazite along fractures in micas (Fig. 7). The mobility of REE, Y, Th and U is related to the fact that many accessories are metamictic and are surrounded by radiation damage structures (see Fig. 12) capable of channelling the migration of REE, Y, Th and U. It is important to emphasize that characteristic accessories from peraluminous granites (monazite, xenotime, huttonite) are inherently more stable than accessories from metaluminous and peralkaline rocks (allanite, thorite).

Effects of the pressure on the composition of major minerals in crustal protoliths

The REEYThU composition of major minerals in amphibolite-grade metasediments and orthogneisses is very similar to that of peraluminous granites. Granulite-grade garnets, however, are noticeably enriched in Nd and Sm and have a larger Eu negative anomaly (Fig. 2). Granulite-grade feldspars

Table 11: Selected analyses of zircon crystals

	1	2	3	4	5	6	7	8	9	10	11*
SiO_2	33·35	34·13	35·04	33·23	34·31	32·38	30·96	31·78	31·30	30·68	28·43
ZrO_2	64·77	62·59	61·97	61·05	63·26	63·03	53·93	60·65	56·76	58·00	53·63
HfO_2	1·97	2·17	1·14	2·29	0·78	1·73	2·31	1·73	1·89	1·35	1·75
Al_2O_3	0·02	0·00	0·00	0·00	0·00	0·40	0·00	0·09	0·01	0·00	0·29
FeO	0·50	0·09	0·83	0·01	0·05	0·18	0·00	0·14	0·04	1·08	0·44
MgO	0·03	0·00	0·05	0·00	0·00	0·02	0·00	0·00	0·00	0·02	0·02
CaO	0·00	0·01	0·16	0·01	0·00	0·17	0·01	0·02	0·02	0·01	0·06
Na_2O	0·00	0·07	0·07	0·00	0·07	0·00	0·00	0·01	0·03	0·10	0·12
P_2O_5	0·01	0·06	0·00	0·53	0·34	1·11	1·79	1·71	2·79	3·16	2·48
					percent						
Y	77·0	199	139	1228	0·70	0·64	2·38	1·74	2·52	3·31	0·79
Th	159	105	259	1011	0·21	0·00	0·66	0·10	0·24	0·08	0·00
U	12·2	54·5	28·1	104	0·00	0·11	5·67	0·88	2·82	0·00	0·22
La	2·60	5·57	1·65	9·52	0·00	0·01	0·01	0·00	0·00	0·01	0·02
Ce	7·75	13·	5·37	26·9	0·03	0·01	0·05	0·01	0·02	0·01	0·03
Pr	1·13	2·84	0·50	4·66	0·01	0·00	0·01	0·00	0·00	0·00	0·01
Nd	5·11	13·3	3·34	29·5	0·03	0·01	0·05	0·01	0·03	0·01	0·05
Sm	1·43	2·48	2·45	15·6	0·03	0·03	0·02	0·01	0·03	0·01	0·03
Eu	0·32	0·53	1·15	4·02	0·01	0·00	0·00	0·00	0·00	0·00	0·00
Gd	1·94	3·74	8·90	42·4	0·04	0·06	0·10	0·04	0·12	0·03	0·05
Tb	0·48	0·81	4·41	14·7	n.d.	n.d.	n.d.	n.d.	n.d.	n.d.	n.d.
Dy	5·42	9·04	47·3	157	0·09	0·07	0·15	0·13	0·22	0·20	0·09
Ho	2·23	3·75	19·0	64·4	n.d.	n.d.	n.d.	n.d.	n.d.	n.d.	n.d.
Er	9·96	20·1	82·5	357	0·08	0·16	0·29	0·22	0·36	0·43	0·11
Tm	2·84	4·05	20·4	73·0	n.d.	n.d.	n.d.	n.d.	n.d.	n.d.	n.d.
Yb	27·8	30·9	188	510	0·17	0·18	0·28	0·37	0·44	0·48	0·13
Lu	9·18	3·73	27·1	69·3	0·04	0·02	0·04	0·10	0·06	0·08	0·04

*Contains 10·05% Sc_2O_3.

REE, Y, Th and U were determined by LA–ICP-MS in samples 1–4 and are expressed in p.p.m. All the other data were obtained by electron microprobe and are expressed in percent. 1, Peraluminous leucogranite (Boquerones); 2, quartz syenite (Magnitogorsk); 3, plagiogranite (Chernoistochinsk); 4, peralkaline granite (Galiñeiro); 5, peralkaline granite (Magnitogorsk); 6, granodiorite (Vierkisest); 7, kinzigite (Ronda); 8, cordierite-bearing granodiorite (Hoyos); 9, xenotime-rich leucogranite (Ronda); 10, xenotime-rich migmatite leucosome (Peña Negra); 11, xenotime-rich granite (Albuquerque). n.d., not determined.

also appear enriched in LREE (Fig. 1), although not as much as garnets. As no changes in LREE composition of major minerals have been found related to increasing temperature (e.g. REE patterns in garnets from biotite gneisses and sanidine-bearing peraluminous dacites are very similar), the increasing pressure seems, in principle, to be mainly responsible for the above-mentioned LREE enrichment in granulite-grade feldspars and garnets. Additional evidence about the role of increasing pressure may be gathered from Harris *et al.* (1992), whose ion-probe data on plagioclase and garnet from a kyanite schist and a sillimanite gneiss also revealed consistently high values of LREE in minerals from the higher-pressure rock.

Much systematic work, not only geochemical but also experimental and crystallographic, is still needed to discover the extension of this phenomenon and the reasons for its occurrence. However, we tentatively suggest that one potentially important mechanism may be the destabilization of monazite by reaction with garnet, which basically consists in

Table 12: Selected LA–ICP-MS analyses of apatite crystals

	Peraluminous						Metaluminous			Peralkaline		
	1	2	3	4	5	6	1	2	3	1	2	3
Y	1806	2467	1486	984	1736	1598	632	951	1024	257	317	284
U	41·1	551	394	0·51	828	129	11·1	35·9	88·7	4·3	15·3	18·1
Th	9·86	14·9	0·61	0·93	81·4	40·7	0·70	2·45	3·17	12·7	46·1	18·0
La	480	630	329	297	444	463	26·2	25·9	60·4	2721	2755	2829
Ce	1452	1709	1156	1181	1632	1659	103	96·6	177	4710	4692	6930
Pr	308	291	198	212	294	295	24·6	31·1	43·6	466	536	656
Nd	1633	1537	865	769	1412	1269	166	214	300	1220	1643	1701
Sm	591	589	324	264	506	456	102	124	135	189	264	235
Eu	4·69	23·7	12·5	14·6	10·2	8·85	28·4	36·5	44·8	58·8	77·5	84·4
Gd	541	769	359	274	707	652	178	243	221	185	262	207
Tb	100	132	59·2	45·3	126	105	36·3	50·5	44·8	22·5	33·1	26·0
Dy	575	742	322	216	616	569	235	289	320	100	135	107
Ho	110	135	59·8	40·2	109	103	51·9	63·5	74·8	18·3	23·6	18·6
Er	302	362	148	94·5	288	272	153	196	197	43·3	50·5	46·8
Tm	43·6	51·9	20·6	13·6	41·7	41·9	20·3	29·1	29·8	4·71	5·53	5·77
Yb	285	298	116	87·5	269	218	122	152	178	24·1	22·7	34·1
Lu	33·9	39·4	13·9	10·5	41·7	27·2	17·1	24·5	28·4	2·49	2·79	3·37
Eu/Eu*	0·03	0·11	0·11	0·17	0·05	0·05	0·64	0·64	0·79	0·96	0·90	1·17
La_N/Yb_N	1·14	1·43	1·91	2·29	1·11	1·43	0·14	0·11	0·23	76·2	81·9	55·9

From peraluminous granites: 1, cordierite-bearing granodiorite (Hoyos); 2, migmatite (Peña Negra); 3, two-mica granite (Pedrobernardo); 4, leucogranite (Trujillo); 5, U-rich leucogranite (Albuquerque); 6, garnet-bearing granite (Murzinka). From metaluminous granites: 1 and 2, granodiorite (Vierkisest); 3, tonalite (Sirostan). From peralkaline granites: 1–3, granite (Keivy).

Table 13: Selected LA–ICP-MS analyses of primary sphene crystals (results are in p.p.m.)

	1	2	3	4	5	6	7	8	9	10	11	12
Y	1150	1612	2127	1100	217	732	100	245	376	2239	1301	1251
U	0·00	10·5	69·8	19·2	391	157	226	32·3	21·9	65·2	1471	439
Th	166	171	163	161	142	213	219	46·9	110	87·7	3268	278
La	1109	1752	2394	1189	3153	1087	1488	281	561	2135	3547	2942
Ce	3596	6102	9273	4315	8157	3337	4786	987	1861	7552	7908	2819
Pr	790	1256	1778	819	1656	608·	845	182	341	1628	973	452
Nd	3240	5279	7453	3484	6839	2519	3525	831	1427	7773	3017	1384
Sm	788	1367	1994	830	2475	510	707	185	291	2084	569	292
Eu	204	240	300	212	398	140	185	57·5	85·8	346	138	99·8
Gd	606	1107	1390	654	1844	391	534	140	229	1539	621	314
Tb	89·5	134	202	89·8	259	55·1	78·0	19·7	30·7	238	74·0	62·2
Dy	458	698	1003	451	1241	290	417	102	165	1184	415	398
Ho	88·5	130	176	82·8	205	58·1	82·0	19·3	32·2	215	85·2	90·5
Er	251	352	452	227	535	160	240	57·8	89·6	564	266	306
Tm	39·5	51·4	63·4	34·23	71·3	23·8	36·5	8·46	13·7	72·5	41·7	47·8
Yb	265·	336	390	230	410	162	234	57·0	89·4	418	296	310
Lu	36·8	41·4	47·8	32·2	46·4	21·7	31·2	7·9	11·5	40·0	40·4	33·9
Eu/Eu*	0·90	0·60	0·55	0·88	0·57	0·96	0·92	1·09	1·02	0·59	0·71	1·01
La_N/Yb_N	2·82	3·52	4·14	3·49	5·19	4·53	4·29	3·33	4·23	3·45	8·09	6·40

1–6, epidote-bearing metaluminous granites and granodiorites (Vierkisest); 7, metaluminous tonalite (Sirostan); 8 and 9, metaluminous diorite (Burguillos del Cerro); 10, 11 and 12, peralkaline granite (Keivy).

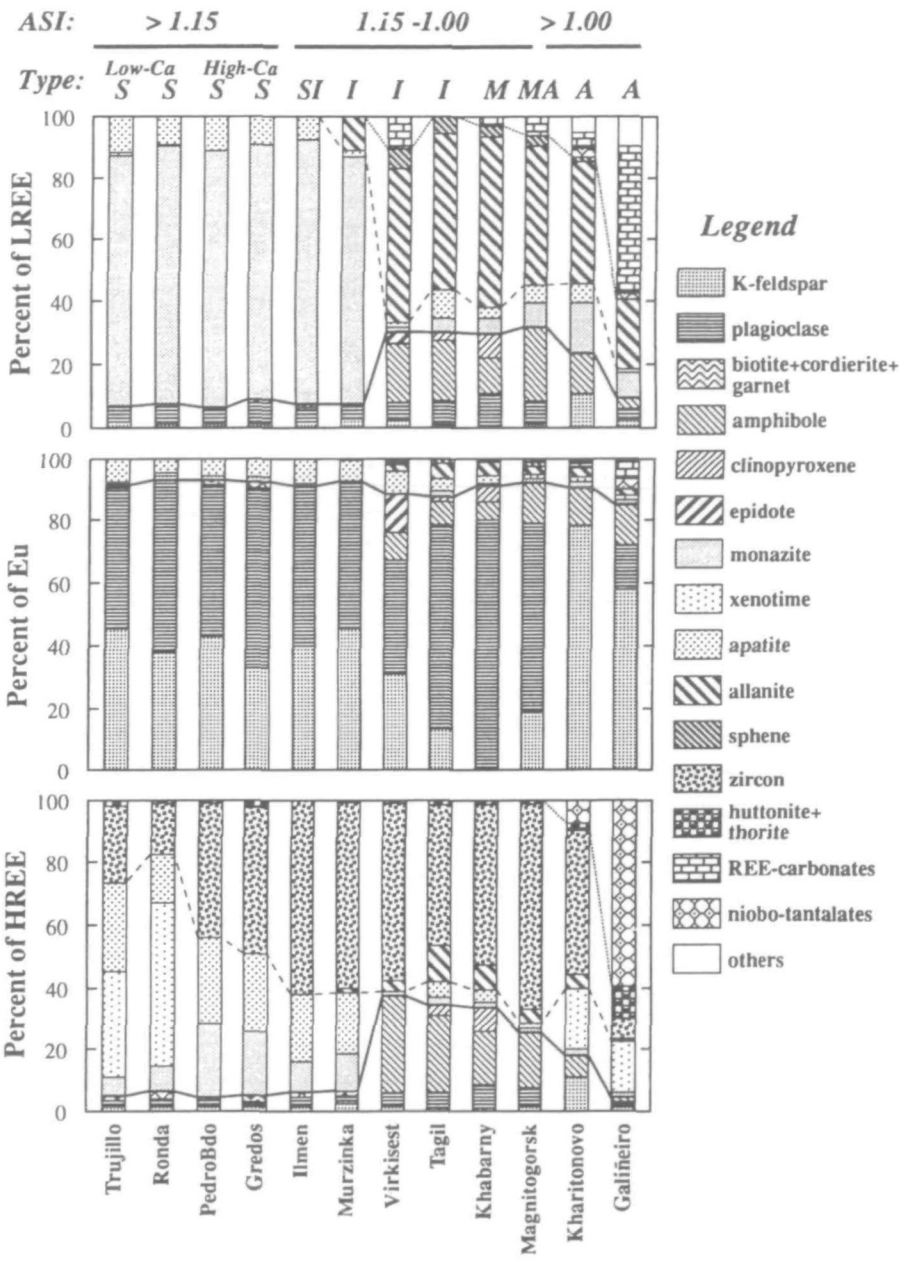

Fig. 17. Fractional contribution of each mineral to the whole-rock LREE, Eu and HREE budgets in selected granite plutons. Continuous line separates the contribution of major from accessory minerals. Dashed line separates the contribution of accessory phosphates from silicates. Dotted line separates accessory silicates from niobotantalates and carbonates. (See discussion in text.)

the exchange of Ca (from garnet) by LREE (from monazite). In a current study on the amphibolite–granulite transition in the Ivrea–Verbano zone (Bea *et al.*, in preparation), we detected that an elevated proportion of monazite grains included within granulite-grade garnets are partially or totally pseudomorphed to a mixture of apatite and cheralite-rich monazite, whereas the garnet around the inclusion is enriched in LREE. Those garnet analyses with abnormally high La–Ce contents reported in Table 5 and Fig. 2 were probably caused by the ablation of such zones.

If pressure-related differences in the REE composition of major minerals are confirmed with more systematic studies, their role as a potential source for differences in the REE chemistry of melts equili-

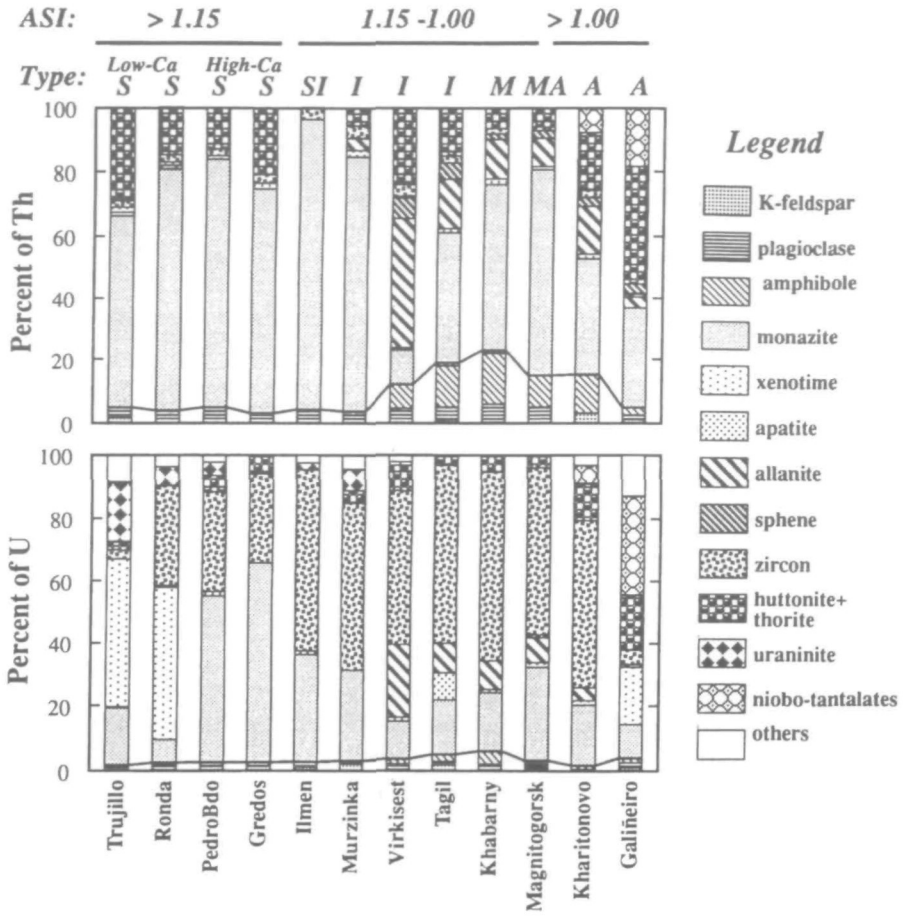

Fig. 18. Fractional contribution of each mineral to the whole-rock Th and U budgets in selected granite plutons. Continuous line separates the contribution of major from accessory minerals. Dashed line separates the contribution of accessory phosphates from silicates. Dotted line separates accessory silicates from niobotantalates and carbonates. (See discussion in text.)

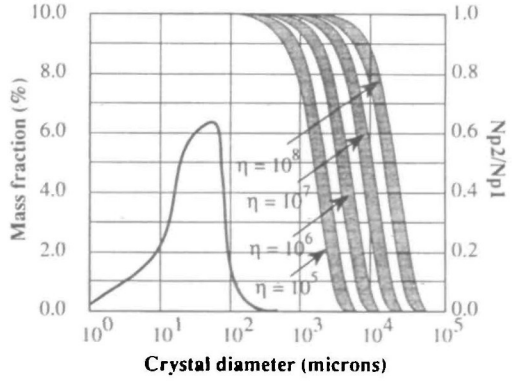

Fig. 19. Settling curves as a function of the diameter of settling minerals calculated with the Bartlett (1969) equation for density intervals between 4 and 6 g/cm^3. The right vertical axis represents the ratio between the mineral particle population densities in the magma near the ceiling (Np_2) and the floor (Np_1). The curve in the left part of the diagram represents the mass fraction of accessories as a function of their diameter. (Note how even 150-μm grains with a density as high as 6 g/cm^3 cannot settle appreciably within a melt with a viscosity as low as 10^5 poises.)

brated at amphibolite- and granulite-grade conditions, respectively, should therefore be considered as a subject for further investigation.

Can REE be used in geochemical modelling of granite rocks?

The objective of trace-element-based petrogenetic modelling of igneous rocks is to infer the behaviour of minerals during melting and crystallization by comparing actual trace-element distribution patterns with theoretical models generally calculated from fractionation equations based on the laws of chemical equilibrium (Allègre & Minster, 1978; Hanson, 1989). To be useful in petrogenetical modelling, a given trace element must be essentially contained within major minerals, obey Raoult–Henry's law, and not move appreciably during post-magmatic stages. It is evident that in the case of granite rocks, REE (except Eu), Y, Th and U do not satisfy any of these conditions and simply cannot

therefore be used for modelling the genesis of granitoids in that manner.

CONCLUSIONS

The LREE, HREE, Y and Th fractions that reside within major minerals are as low as 5–10 wt% in peraluminous and peralkaline granites, but may rise to 20–30 wt% in amphibole-rich metaluminous granites. Eu is always essentially contained within feldspars, although primary epidote may also contain a significant proportion. The fraction of U that resides within major minerals is always <5 wt%.

The geochemistry of REE (except Eu), Y, Th and U in granite rocks and crustal protoliths is essentially controlled by the behaviour of REEYThU-rich accessory minerals, whose nature, associations and composition change with rock aluminosity. The accessory assemblage of peraluminous granites is composed of monazite, xenotime (restricted to low-Ca varieties), apatite, zircon, Th-orthosilicate (huttonite?), uraninite and betafite–pyrochlore minerals. Metaluminous granites have allanite, sphene, apatite, minor monazite, zircon and Th-orthosilicate (thorite?). Peralkaline granites have the same accessories as metaluminous granites, but also contain niobotantalates (aeschinite, samarskite, fergusonite, occasionally loparite), batnaesite, fluocerite and xenotime.

Migmatites and high-grade rocks contain the same accessory assemblage and similar REE, Y, Th and U distribution patterns among minerals as granites with similar aluminosity. Only garnet, owing to its higher abundance, plays a much more important role here, especially for Y and HREE. Compared with the same minerals from amphibolite-grade metapelites, granulitic feldspars are enriched in LREE, above all in La and Ce. In the same way, granulitic garnets have Nd–Sm contents higher by one order of magnitude than amphibolitic garnets and a precipitous negative Eu anomaly.

In common peraluminous migmatites, the mass fraction of monazite, xenotime and zircon included within biotite is very high. Whether these inclusions are available for the melt during anatexis or stay within their host—either in restites or entrained within restitic crystals suspended in the melt—depends completely on the behaviour of biotite. During crystallization, the small grain-size of newly formed accessories makes their separation from the melt physically impossible until a growing major mineral includes them. Biotite, which has near-zero contents of REE, Y, Th and U, is the mineral which shows the greatest tendency to include REEYThU-rich accessories, probably owing to the combined effects of local saturation adjacent to growing biotite crystals and heterogeneous nucleation.

REE, Y, Th and U are not suitable for geochemical modelling of granitoids by means of equilibrium-based trace-element fractionation equations, but are still useful petrogenetic tools. Apart from the obvious importance of Th and U as heat-producing elements, and REE in isotopic systems such as Sm–Nd, Lu–Hf or La–Ba, the geochemistry of REE, Y, Th and U reflects the behaviour of accessories and some key major minerals such as garnet, feldspars and amphibole, and may therefore give valuable information about the conditions of partial melting, melt segregation and crystallization of granite magmas in different crustal regimes.

ACKNOWLEDGEMENTS

I acknowledge with many thanks help from the following people and institutions: P. G. Montero, for her assistance with LA–ICP-MS analyses and fruitful comments and criticism—she also provided me with samples from Galiñeiro; G. B. Fershtater, for his invaluable help during field-work in the Urals and many hours of passionate discussion on granites; G. Garuti and F. Zaccharini, for introducing me to the geology of the Ivrea–Verbano zone and their help with microprobe analyses at Modena University; Isabel and Alicia, for their patience during many hours of tedious studies with the SEM; A. Acosta and L. G. Menéndez, for providing samples from Ronda and Albuquerque; C. Laurin, for her help and patience in improving the original Spanglish manuscript. Revisions made by Gordon Watt, David London and Simon Harley are gratefully acknowledged. Perkin Elmer allowed free use of a new UV-LA probe prototype for ICP-MS analyses. This work has been financially supported by the Spanish Interministry Commission for Science and Technology (CICYT), Projects AMB93-0535 and AMB94-1420.

REFERENCES

Aleinikoff, J. N. & Stoeser, D. B., 1989. Contrasting zircon morphology and U–Pb systematics in peralkaline and metaluminous post-orogenic granite complexes of the Arabian Shield, Kingdom of Saudi Arabia. *Chemical Geology* **79**, 241–258.

Allègre, C. J. & Minster, J. F., 1978. Quantitative models of trace element behavior in magmatic processes. *Earth and Planetary Science Letters* **38**, 1–25.

Bacon, C. R., 1989. Crystallization of accessory phases in magmas by local saturation adjacent to phenocrysts. *Geochimica et Cosmochimica Acta* **53**, 1055–1066.

Barbey, P., Alle, P., Brouand, M. & Albarede, F., 1995. Rare-earth patterns in zircons from the Manaslu granite and Tibetan Slab migmatites (Himalaya): insights in the origin and evolu-

tion of a crustally-derived granite magma. *Chemical Geology* **125**, 1–17.

Bartlett, R. W., 1969. Magma convection, temperature distribution, and differentiation. *American Journal of Science* **267**, 1067–1082.

Bayer, G., 1969. Thorium A. Crystal chemistry. In: Wedepohl, K. H. (ed.) *Handbook of Geochemistry*. Heidelberg: Springer-Verlag.

Bea, F., 1993. Aluminosity-dependent fractionation patterns in differentiated granite–leucogranite systems. *EOS* **74**(16), 343.

Bea, F., Fershtater, G. & Corretgé, L. G., 1992. The geochemistry of phosphorus in granite rocks and the effect of aluminium. *Lithos* **29**, 43–56.

Bea, F., Pereira, M. D., Corretgé, L. G. & Fershtater, G. B., 1994*a*. Differentiation of strongly peraluminous, perphosphorous granites. The Pedrobernardo pluton, central Spain. *Geochimica et Cosmochimica Acta* **58**, 2609–2628.

Bea, F., Pereira, M. D. & Stroh, A., 1994*b*. Mineral/leucosome trace-element partitioning in a peraluminous migmatite (a laser ablation–ICP-MS study). *Chemical Geology* **117**, 291–312.

Chesner, C. A. & Ettlinger, A. D., 1989. Composition of volcanic allanite from Toba Tuffs, Sumatra, Indonesia. *American Mineralogist* **74**, 750–758.

Delima, E. S., Vannucci, R., Bottazzi, P. & Ottolini, L., 1995. Reconnaissance study of trace element zonation in garnet from the Central Structural Domain, Northeastern Brazil: an example of polymetamorphic growth. *Journal of South American Earth Sciences* **8**, 315–324.

Drake, M. J. & Weill, D. F., 1972. New rare earth element standards for electron microprobe analysis. *Chemical Geology* **10**, 179–181.

Förster, H. J., 1993. Th–Y–REE-bearing accessory minerals in Hercynian granites of the Erzgebirge (Ore Mountains), Germany. *Geological Society of America, Abstracts with Programs* **25**, 42–43.

Förster, H. J. & Rhede, D., 1995. Extreme compositional variability in granitic monazites. In: Brown, M. & Piccoli, P. M. (eds) *Third Hutton Symposium on the Origin of Granites and Related Rocks*, College Park, MD. *US Geological Survey Circular* **1129**, 54–55.

Förster, H. J. & Tischendorf, G., 1994. Evolution of the Hercynian granite magmatism in the Erzegebirge metallogenic provinces. *Mineralogical Magazine* **58A**, 284–285.

Gromet, L. P. & Silver, L. T., 1983. Rare earth element distribution among minerals in a granodiorite and their petrogenetic implications. *Geochimica et Cosmochimica Acta* **47**, 925–940.

Hanson, G. N., 1989. An approach to trace element modeling using a simple igneous system as an example. In: Lipin, B. R. & McKay, G. A. (eds) *Geochemistry and Mineralogy of REE. Mineralogical Society of America, Reviews in Mineralogy* **21**, 79–97.

Harris, N. B. W., Gravestock, P. & Inger, S., 1992. Ion-microprobe determinations of trace-element concentration in garnets from anatectic assemblages. *Chemical Geology* **100**, 41–49.

Haskin, L. A., 1979. On rare-earth element behavior in igneous rocks. In: Ahrens, L. H. (ed.) *On Rare-Earth Element Behavior in Igneous Rocks*. Oxford: Pergamon, pp. 175–189.

Haskin, L. A., 1990. PREEconceptions pREEvent pREEcise pREEdictions. *Geochimica et Cosmochimica Acta* **54**, 2353–2361.

Heaman, L. & Parrish, R., 1991. U–Pb geochronology of accessory minerals. In: Heaman, L. & Ludden, J. N. (eds) *Short Course Handbook on Applications of Radiogenic Isotope Systems to Problems in Geology*. Toronto, Ont.: Mineralogical Association of Canada, pp. 59–102.

Heaman, L. M., Bowis, R. & Crocket, J., 1990. The chemical composition of igneous zircon suites: implications for geochemical tracer studies. *Geochimica et Cosmochimica Acta* **54**, 1597–1608.

Hickmott, D. D. & Shimizu, N., 1990. Trace element zoning in garnet from the Kwoick Area, British Columbia: disequilibrium partitioning during garnet growth? *Contributions to Mineralogy and Petrology* **104**, 619–630.

Hickmott, D. D., Shimizu, N., Spear, F. S. & Selverstone, J., 1987. Trace-element zoning in a metamorphic garnet. *Geology* **15**, 573–576.

Imaoka, T. & Nakashima, K., 1994. Fluocerite in a peralkaline rhyolite dyke from Cape Ashizuri, Shikoku-Island, Southwest Japan. *Neues Jahrbuch für Mineralogie, Monatshefte* **12**, 529–539.

Krasnobayev, A. A., 1986. *Zircon kak indikator geologicheskij prozessov*. Moscow: Nauka.

Lanzirotti, A., 1995. Yttrium zoning in metamorphic garnets. *Geochimica et Cosmochimica Acta* **59**, 4105–4110.

London, D., 1992. Phosphorus in S-type magmas: the P_2O_5 content of feldspars from peraluminous granites, pegmatites, and rhyolites. *American Mineralogist* **77**, 126–145.

Mazzuchelli, M., Rivalenti, G., Vannucci, R., Botazzi, P., Ottolini, L., Hoffmann, A. W. & Parenti, M., 1992. Primary positive Eu anomaly in clinopyroxenes of low-crust gabbroic rocks. *Geochimica et Cosmochimica Acta* **56**, 2363–2370.

McKay, G. A., 1989. Partitioning of rare earth elements between major silicate minerals and basaltic melts. In: Lipin, B. R. & McKay, G. A. (eds) *Geochemistry and Mineralogy of REE. Mineralogical Society of America, Reviews in Mineralogy* **21**, 45–77.

Miller, C. F. & Mittlefehdlt, D. W., 1982. Light rare earth element depletion in felsic magmas. *Geology* **10**, 129–133.

Montero, P. G., 1995. Accumulation of REE and HFS elements in peralkaline granitoids: the Galiñeiro pluton, NW Spain. In: Brown, M. & Piccoli, P. M (eds) *Third Hutton Symposium on the Origin of Granites and Related Rocks*, College Park, MD. *US Geological Survey Circular* **1129**, 98–99.

Petrik, I., Broska, I., Lipka, J. & Siman, P., 1995. Granitoid allanite-(Ce): substitution relations, redox conditions and REE distributions (on an example of I-type granitoids, Western Carpathians, Slovakia). *Geologica Carpathica* **46**, 79–94.

Pichavant, M., Montel, J. M. & Richard, L. R., 1992. Apatite solubility in peraluminous liquids: experimental data and an extension of the Harrison–Watson model. *Geochimica et Cosmochimica Acta* **56**, 3855–3861.

Pupin, J. P., 1980. Zircon and granite petrology. *Contributions to Mineralogy and Petrology* **73**, 207–220.

Pupin, J. P., 1992. Les zircons des granites océaniques et continentaux: couplage typologie–géochimie des éléments en traces. *Bulletin Société géologique du France* **163**, 495–507.

Rapp, R. P. & Watson, E. B., 1986. Monazite solubility and dissolution kinetics: implications for the thorium and light rare earth chemistry of felsic magmas. *Contributions to Mineralogy and Petrology* **94**, 304–316.

Reid, M. R., 1990. Ionprobe investigation of rare earth elements distribution and partial melting of metasedimentary granulites. In: Vielzeuf, D. & Vidal, P. (eds) *Granulites and Crustal Evolution*. Dordrecht: Kluwer Academic, pp. 506–522.

Reischmann, T., Brugmann, G. E., Jochum, K. P. & Todt, W. A., 1995. Trace element and isotopic composition of baddeleyite. *Mineralogy and Petrology* **53**, 155–164.

Roeder, P. L., 1985. Electron-microprobe analysis of minerals for rare-earth elements: use of calculated peak-overlap corrections. *Canadian Mineralogist* **23**, 263–371.

Roeder, P. L., MacArthur, D., Ma, X. P. & Palmer, G. R., 1987. Cathodoluminescence and microprobe study of rare-earth elements in apatite. *American Mineralogist* **72**, 801–811.

Rub, V. G., Rub, A. K. & Salmin, Y. P., 1994. On the peculiarities of REE and some trace elements in the zircons of ore-bearing granites. *Geokhimiya* **11**, 1577–1590.

Rubin, J., Henry, C. D. & Price, J. G., 1989. Hydrothermal zircons and zircon overgrowths, Sierra Blanca Peaks, Texas. *American Mineralogist* **74**, 865–869.

Sawka, W. N., 1988. REE and trace element variations in accessory minerals and hornblende from the strongly zoned McMurry Meadows Pluton, California. *Transactions of the Royal Society of Edinburgh: Earth Sciences* **79**, 157–168.

Sawka, W. N. & Chappell, B. W., 1988. Fractionation of uranium, thorium and rare earth elements in a vertically zoned granodiorite: implications for heat production distribution in the Sierra Nevada batholith, California, U.S.A. *Geochimica et Cosmochimica Acta* **52**, 1131–1144.

Sevigny, J. H., 1993. Monazite controlled Sm/Nd fractionation in leucogranites: an ion microprobe study of garnet phenocrysts. *Geochimica et Cosmochimica Acta* **57**, 4095–4102.

Tourrette, T. Z. L., Burnett, D. S. & Bacon, C. R., 1991. Uranium and minor-element partitioning in Fe–Ti oxides and zircon from partially melted granodiorite, Crater Lake, Oregon. *Geochimica et Cosmochimica Acta* **55**, 457–470.

Vlasov, K. A., 1966. *Geochemistry and Mineralogy of Rare Elements and Genetic Types of their Deposits*. Jerusalem: Israel Program for Scientific Translation.

Wark, D. A. & Miller, C. F., 1993. Accessory mineral behavior during differentiation of a granite suite: monazite, xenotime, and zircon in the Sweetwater Wash pluton, southeastern California. *Chemical Geology* **110**, 49–67.

Watson, E. B., 1988. The role of accessory minerals in granitoid geochemistry. In: *First Hutton Meeting on the Origin of Granite and Related Rocks, Vol. 1*. Edinburgh: Royal Society of Edinburgh, pp. 19–20.

Watson, E. B. & Harrison, T. M., 1984. Accessory minerals and the geochemical evolution of crustal magmatic systems: a summary and prospectus of experimental approaches. *Physics of the Earth and Planetary Interiors* **35**, 19–30.

Watson, E. B., Vicenzi, E. P. & Rapp, R. P., 1989. Inclusion/host relations involving accessory minerals in high-grade metamorphic and anatectic rocks. *Contributions to Mineralogy and Petrology* **101**, 220–231.

Watt, G. R. & Harley, S. L., 1993. Accessory phase controls on the geochemistry of crustal melts and restites produced during water-undersaturated partial melting. *Contributions to Mineralogy and Petrology* **114**, 550–556.

Wolf, M. B. & London, D., 1994. Apatite dissolution into peraluminous haplogranitic melts: an experimental study of solubilities and mechanisms. *Geochimica et Cosmochimica Acta* **58**, 4127–4146.

Wolf, M. B. & London, D., 1995. Incongruent dissolution of REE- and Sr-rich apatite in peraluminous granitic liquids: differential apatite, monazite, and xenotime solubility during anatexis. *American Mineralogist* **80**, 765–775.

Yurimoto, H., Duke, E. F., Papike, J. J. & Shearer, C. K., 1990. Are discontinuous chondrite-normalized REE patterns in pegmatite granite systems the results of monazite fractionation? *Geochimica et Cosmochimica Acta* **54**, 2141–2145.

RECEIVED JUNE 20, 1995
REVISED TYPESCRIPT ACCEPTED DECEMBER 8, 1995